Methods to measure characteristics of mirror facets of Imaging Atmospheric Cherenkov Telescopes

Diploma Thesis of

Anneli Schulz

from Villingen-Schwenningen, Germany

performed at the
ECAP
(University of Erlangen-Nuremberg)
Erwin-Rommelstr. 1, 91058 Erlangen

supervisor:
Prof. Dr. Christian Stegmann
second reader:
Prof. Dr. Uli Katz

5. November 2010

Abstract

In this thesis different mirror facets for the telescopes in the upcoming Cherenkov Telescope Array (CTA) are investigated. To develop a reliable test for the characterization of the different prototypes, currently designed at different universities, two approaches are presented here. The first method is an optical imaging method, the so-called $2f$-setup, which has already been used to characterize mirrors of currently working telescopes. The second method is a completely new approach, namely Phase Measuring Deflectometry (PMD) which was developed by the OSMIN group in Erlangen. It proved to be very successful in measuring eyeglasses but was used to characterize mirror facets in the frame of this thesis for the first time. Besides measurements with both techniques, a ray tracing program was developed to transform the PMD results into a point-spread-function, which is needed to compare both methods. The results show a good correlation of the two strategies. Using both methods on four CTA mirror prototypes, it could be shown that only one of them satisfies the quality requirements for CTA, but that all production techniques are showing great potential to produce excellent mirrors.

Zusammenfassung

In dieser Arbeit werden verschiedene Spiegel-Facetten für Teleskope des geplanten Cherenkov Telescope Arrays (CTA) untersucht. Für die Entwicklung zuverlässiger Tests zur Charakterisierung der unterschiedlichen Prototypen, die momentan an verschiedenen Universitäten hergestellt werden, werden in dieser Arbeit zwei verschiedene Ansätze vorgestellt. Der erste Ansatz ist eine abbildende optische Methode, der sogenannte $2f$-Aufbau, der schon für die Spiegelvermessung bestehender Teleskope verwendet wurde. Der zweite Ansatz ist die Phasenmessende Deflektometrie (PMD), die von der OSMIN Gruppe in Erlangen entwickelt wurde und im Rahmen dieser Arbeit das erste Mal zur Vermessung von Spiegel-Facetten eingesetzt wurde. Neben der Durchführung von Messungen mit beiden Verfahren wurde ein Raytracing-Programm entwickelt um die Ergebnisse der PMD-Messung in eine Punktverbreiterungsfunktion zu transformieren. Dies ist notwendig um die beiden Messungen vergleichen zu können. Es zeigte sich eine gute Übereinstimmung beider Methoden. Bei der Verwendung beider Techniken zur Charakterisierung von vier CTA Spiegel-Prototypen konnte gezeigt werden, dass nur einer von ihnen die Voraussetzungen für CTA erfüllt, aber alle Produktionstechniken das Potential haben exzellente Spiegel herzustellen.

Contents

1. Introduction

The night sky filled with stars has always been fascinating to mankind. The celestial bodies will follow their pathways no matter what mankind will do, making them a symbol for the things mankind can not influence and hardly grasp. The quest to understand the underlying laws and mechanisms has aroused the curiosity of astronomers for centuries and millennia. Deliberations that the Earth is round and that the moon is bright only because the Sun is shining on it have been made by Thales of Miletus 600 BC, subsequently he predicted the solar eclipse in 585 BC correctly. But it took another 2000 years until the modern heliocentric world view was established by Nicolaus Kopernicus (1473 – 1543) in his main work "De Revolutionibus Orbium Coelestium Libri VI". Influenced by the work of Kopernicus the German mathematician Johannes Kepler (1571 – 1630) analysed the remarkably precise measurements of Tycho Brahe. This led him to the famous laws of planetary motion, which included non circular trajectories of the planetary bodies for the first time. All these results and knowledge were gained by viewing the sky with the unaided eye only. The invention of the telescope and its use to astronomy by Galileo Galilei (1564 - 1642) opened a whole new world of possibilities. He discovered crater and other mountain ranges on the moon and the Jupiter moons. This was the advent of modern astronomy, a research field which is still growing and leading to completely new results today.

Astronomy started with observations in the optical part of the electromagnetic spectrum, but with the help of new technical possibilities nowadays photons in all parts of the electromagnetic spectrum can be detected. The electromagnetic spectrum, reaching from the high energetic γ-rays via optical light to low energy radio waves, is shown in Fig. 1.1. Astronomers in the different regimes of the spectrum use different characteristic variables to describe the properties of the observed photons: radio astronomers utilize the frequency ν, optical astronomers use the wavelength λ, while X-and γ-rays are usually expressed in energies E. The wavelength, the frequency and the energy are equivalent

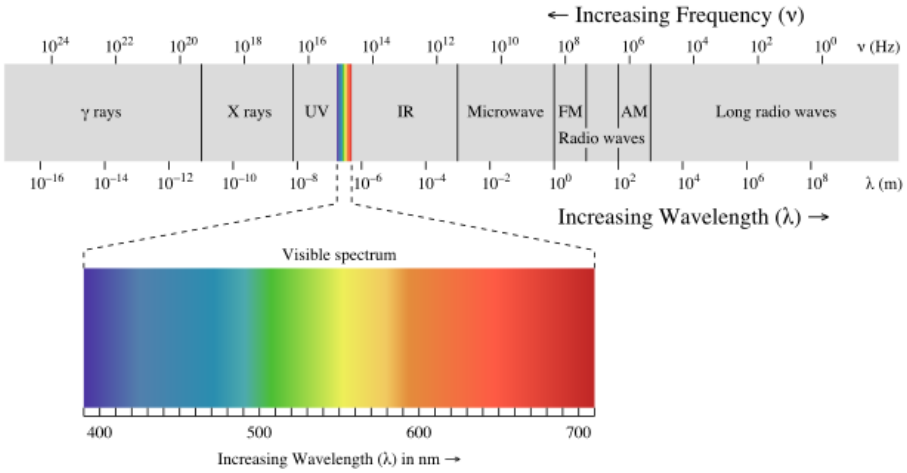

Figure 1.1.: The electromagnetic spectrum reaching from γ-rays to radio waves, radio-photons have the longest wavelength and the lowest energies, while γ-rays have the shortest wavelength and the highest energies.

descriptions of the photon properties, the relations between them are:

$$\mathrm{E} = h \cdot \nu, \qquad \nu = \frac{\mathrm{E}}{h}, \qquad \lambda = \frac{c}{\nu} \tag{1.1}$$

where $c = 2.99792458 \times 10^8\,\mathrm{m/s}$ is the speed of light in vacuum and $h = 4.13566733 \times 10^{-15}\,\mathrm{eV}$ is Planck's constant. Most of the open questions in astronomy can only be answered if one source is observed at different wavelengths, in so-called multi-wavelength observations. In the future it might even be possible to do astronomy also with neutrinos.

The detection technique for photons with different energies depends on the opacity of the Earth's atmosphere, which is shown in the upper panel of Fig. 1.2. Radio and optical astronomy are ground based techniques, since the Earth's atmosphere is transparent for photons with these energies. Photons with other wavelengths, e.g infrared, X-rays and γ-rays, are absorbed by the atmosphere and therefore have to be observed from space. Even though the atmosphere is also opaque to photons with energies $\geq 100\,\mathrm{GeV}$, earth-bound observations of these photons are possible when using the whole atmosphere as detector. Thereby Cherenkov flashes are observed, which are emitted by secondary particles from airshowers induced by very high energetic photons. The flux of photons at the Very High Energies (VHE, $E_\gamma \geq 100\,\mathrm{GeV}$) is below one particle per km^2 and year. This is the reason for the need of large detectors, which cannot be brought to space. The details of this detection technique used by so-called Imaging Air Cherenkov Telescopes

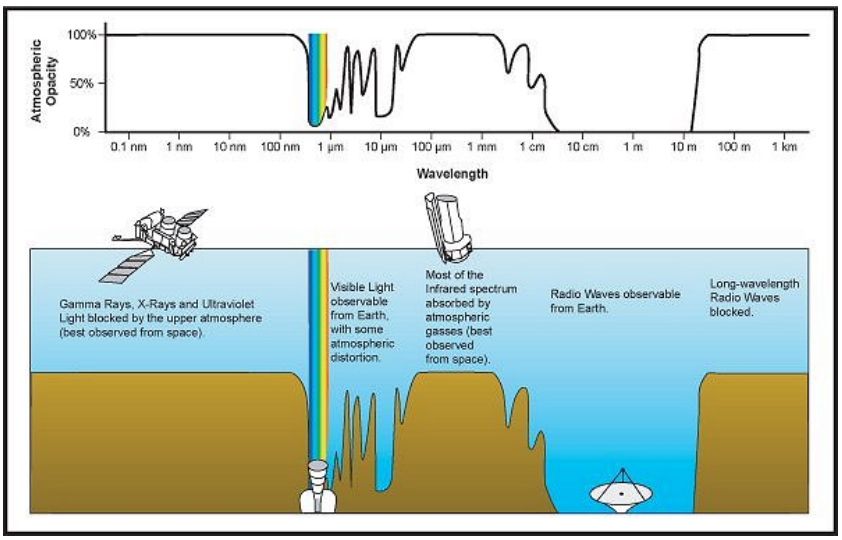

Figure 1.2.: The atmospheric opacitiy for the electromagnetic spectrum reaching from γ rays to radio waves. The upper panel shows the atmospheric opacity as a function of wavelength, if the opacity is 100 % the photons do not reach the ground, if the opacity is 0 % all photons reach the ground. The lower panel shows the different detector types and their location. Credit for this picture: NASA/IPAC.

(IACT) are described in Chapter 2. The imaging atmospheric Cherenkov technique is a very successful method to observe at such high energies.

The H.E.S.S. telescope array, consisting of four IACT-telescopes, is situated in the Khomas highland in Namibia. It is one of the most successful IACTs. Figure 1.3 shows a picture of one of the H.E.S.S. telescopes. The main purpose of a IACT-telescope is, like for all telescopes, to focus light onto a camera. Consequently mirrors are an essential part of IACTs. These mirrors have to fulfil certain specifications, the reflectivity has to be high enough and they have to focus the light into a small spot. The criteria for the mirrors are outlined in Chapter 2. Before the mirrors are mounted onto the telescopes they need to be checked thoroughly to ensure proper operation. This is the main topic of this thesis. Until now only optical imaging methods, where the picture of a light source after the reflection on the mirror is observed, were used to check the properties of these mirrors. The $2f$ method is one where the light source and the camera both are at a distance of $2f$ from the mirror facet. It is described in Chapter 3, particularly the layout of our own setup and systematic studies with different light sources and detectors are elucidated. The advantages of the $2f$ method are its easiness and cheapness, but the

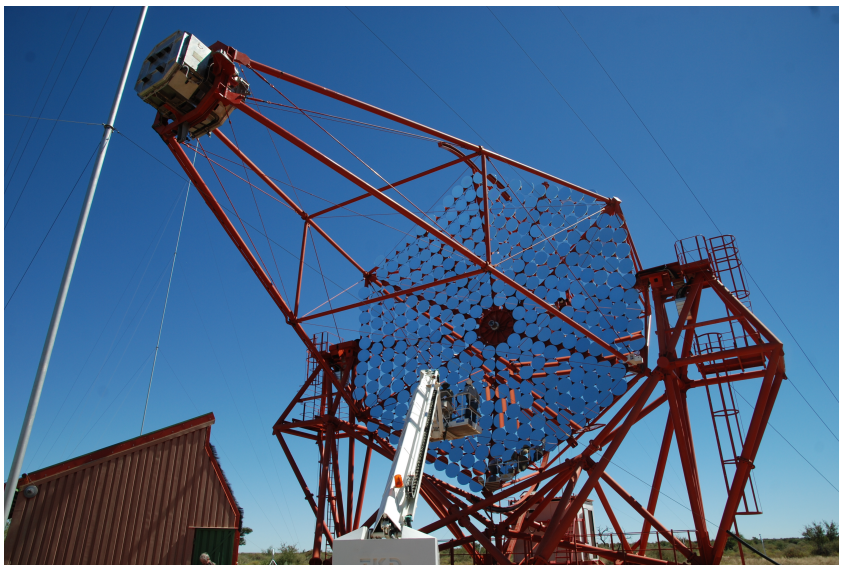

Figure 1.3.: This picture shows one of the telescopes of the H.E.S.S. array situated in the Khomas highland in Namibia. Note that the picture was taken directly after mirror exchange and therefore the mirror facets are not yet aligned.

problem is that the distance always has to be twice the focal length, leading to large setups. In this thesis an alternative method to examine the properties of the mirrors is also presented: Phase Measuring Deflectometry (PMD). It is described in Chapter 4, starting with an explanation of the measuring principle followed by the measurements. It is more sophisticated than the $2f$ setup and has the advantage of the possibility to obtain more detailed information about the mirror's surface and a more compact setup. The comparison of the results of the two different methods is done in Chapter 5. Chapter 6 contains the conclusion and outlook.

2. Imaging Air Cherenkov Telescopes

In this chapter IACTs and the physics they are based on are described. The energy range of the existing IACTs is from $\approx$ 100 GeV up to several TeV. Amazing results were gathered using IACTs, which are based on the imaging atmospheric Cherenkov technique described in Sect. 2.1. In Sect. 2.2 an outline of the Cherenkov Telescope Array, which is currently designed, is given. Sect. 2.3 describes different approaches to fabricate mirror facets.

2.1. The imaging atmospheric Cherenkov technique

If Very High Energetic γ (VHE, $E_\gamma \geq 100\,\mathrm{GeV}$) or nuclei hit the atmosphere of the Earth, they are not able to penetrate through but they collide with molecules (mainly N_2 and O_2) and produce a cascade of secondary particles. In the case of incident photons an electromagnetic shower is formed, if the incident particle was a nucleus a hadronic shower results. Most of the secondary particles travel faster than the speed of light in the atmosphere. If particles travel faster than the waves they send out, the waves interfere constructively and produce a cone of light, the so-called Cherenkov-light, which has a characteristic opening angle θ_c. Using Fig. 2.1 it is easy to see that the opening angle of the cone is defined by the distances the particle and the light travel during a time interval t. Light travels at a speed of $c_n = \frac{c_0}{n}$ with the refraction index n and the particle at a speed v, and with $\beta = \frac{v}{c_0} \Rightarrow v = \beta \cdot c_0$, the opening angle can be calculated in the following way:

$$\cos\theta_c = \frac{c_n \cdot t}{v \cdot t} = \frac{c_0/n\, t}{\beta c_0\, t} = \frac{1}{\beta n}.$$

As shown for example in Giavitto (2007) and Elfahem (1999) the spectrum of the Cherenkov light is proportional to $1/\lambda^2$ with the wavelength λ. The spectrum has a maximum at about $\lambda = 330\,\mathrm{nm}$ since scattering and absorption processes conceal the

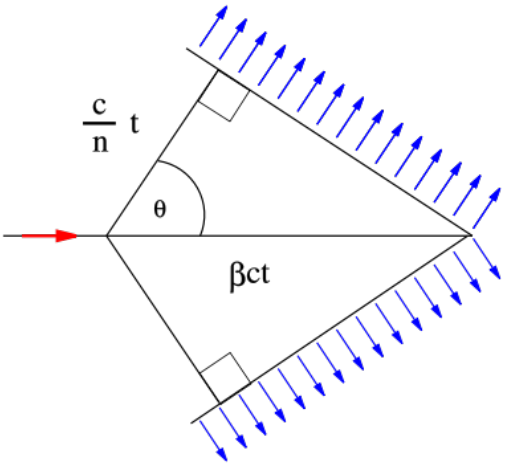

Figure 2.1.: Sketch of the Cherenkov cone of a particle travelling at a speed $v = \beta \cdot c$.

shorter wavelengths. A γ-ray with an initial energy of 1 TeV leads to $\sim 100\,\mathrm{photons/m^2}$ at 2000 m above sea level. The duration of the Cherenkov flash is $5 - 20\,\mathrm{ns}$ (Hinton, 2009).

To detect Cherenkov light emitted by air shower particles optical telescopes are used. Their mirrors reflect the light onto a photomultiplier camera positioned at the focal point of the mirrors. All rays of light with same angles with respect to the mirror surface are reflected onto the same point in the camera. The different positions in the camera correspond to different angles of the incoming rays and an image of the air shower is obtained, hence the name *imaging* atmospheric Cherenkov telescopes. Due to the low photon fluxes of the Cherenkov light large collecting areas ($> 100\,\mathrm{m^2}$) are needed, which can only be obtained using segmented mirrors. Additionally observations are only possible during dark and clear nights.

The picture of an airshower in the camera is usually elliptical, the longitudinal dimension of the shower is larger than the transversal one. The axis of the shower is a straight line in the camera picture pointing to the direction of the initial photon and consequently the direction of the γ-ray source. The imaging of the air shower in the camera is shown in Fig. 2.2(a). To use the Cherenkov telescope in an ideal way it is necessary that the angular resolution of the mirror facets is smaller than one camera pixel, i.e., 0.1 mrad. The first successes using IACTs were made by the Whipple collaboration, which detected the Crab Nebula as the first source emitting TeV γ-rays in 1989 (see Weekes et al., 1989). Nowadays the Crab Nebula is used as a standard candle in γ astronomy, the current instruments can detect sources with $< 1\%$ of the flux of the Crab Nebula and the

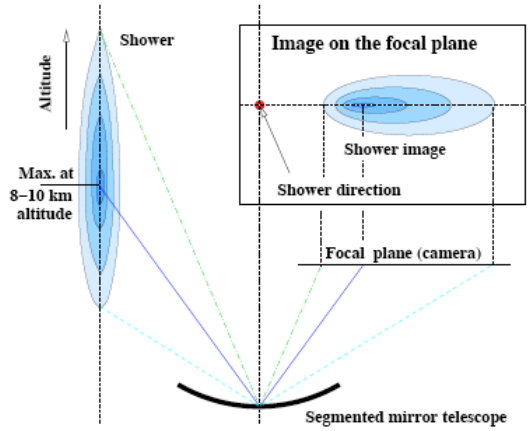

(a) Sketch showing the detection technique of IACTs, the light from the shower gets focussed onto the camera.

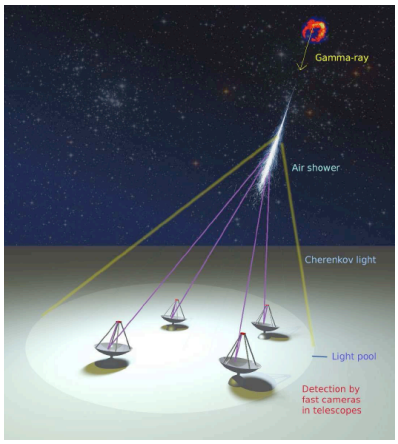

(b) Schematic view of the Cherenkov cone emitted by air shower particles

Figure 2.2.: Schematic views showing the detection of Cherenkov photons with IACTs, pictures from Antonelli et al. (2009).

number of sources with TeV γ emission has grown to over 100[1]. Although an enhanced γ-ray flux from the Crab Nebula region in the MeV regime has been seen by Agile (The Astronomer's Telegram, ATel No. 2855)[2] and confirmed by Fermi LAT (ATel No. 2861) in September 2010, there are until now no indications for variation in the TeV energy regime. Neither MAGIC (ATel No. 2967) nor VERITAS (ATel No. 2968) found evidence for an enhanced flux from the Crab Nebula region.

The HEGRA experiment has shown that there are several advantages of using an array of IACTs. One advantage is that if two telescopes observe the same airshower it is possible to get the direction of the shower by the intersection of the shower axes, this leads to a higher accuracy in the determination of the shower origin. Fig. 2.2(b) shows the Cherenkov cone illuminating four telescopes on the ground, the axes of the reconstructed air shower all point to the origin of the airshower. The scan of the galactic plane by the H.E.S.S. collaboration (Aharonian et al., 2006; Chaves, 2009) was a great success and many new TeV sources were discovered.

At the moment there are different collaborations working on IACTs, the H.E.S.S. collaboration with four telescopes in Namibia, the MAGIC collaboration with two telescopes

[1]The current number of TeV sources can be found in the TeV catalog by S. Wakely, D. Horan published at http://tevcat.uchicago.edu.

[2]The Astronomer's Telegrams can be found at http://www.astronomerstelegram.org.

Table 2.1.: Characteristics of currently operating IACTs and IACT arrays. *Lat.* and *Long.* stand for the geographical coordinates of the observation sites. *Tels.* gives the number of telescopes, the *total area* is the sum of the collecting areas of all telescopes in the array. *Pixels* denotes the number of camera pixels. The *FoV* is the field of view and *thresh.* the threshold energy for a detection. The approximate *sensitivity* is expressed as the minimum flux (as a percentage of that of the Crab Nebula: $\approx 2 \times 10^{-11}$ photons cm^{-2} s^{-1} above 1 TeV) of a point-like source detectable at the 5σ significance level in a 50 hour observation. Adopted from Hinton (2009).

Instrument	Lat. (°)	Long. (°)	Tels.	Total Area (m^2)	Pixels	FoV (°)	Thresh. (GeV)	Sensitivity (% Crab)
H.E.S.S.	-23	16	4	428	960	5	100	0.7
VERITAS	32	-111	4	424	499	3.5	100	1
MAGIC	29	18	1	234	574	3.5	60	2
CANGAROO-III	-31	137	3	172	427	4	400	15
Whipple	32	-111	1	75	379	2.3	300	15
HEGRA	29	18	5	43	271	4.3	500	5

in La Palma, VERITAS with four telesopes in Arizona, USA, and CANGAROO in Australia. A summary of the existing IACTs can be found in table 2.1.

2.2. The Cherenkov Telescope Array (CTA) observatory

The great potential of γ-ray astronomy has been shown by the results of the existing IACTs, but to explore the universe even deeper a larger detection area is needed. The following paragraph summarises the CTA design report by the CTA Consortium (2010). CTA will start the next generation of IACTs with unprecedented sensitivity and resolution. The number of telescopes will be around 100 and the sensitivity will be one order of magnitude higher than the best of the current instruments. The large detection area will lead to much higher detection rates and CTA will therefore be able to investigate also transient phenomena. It will cover the energy range from some 10 GeV to beyond 100 TeV photon energy uniformly. The improved angular resolution will make it possible to study the morphology of extended sources. The main scientific goals are to understand the origin of cosmic rays, the nature of particle acceleration, and to search for physics beyond the standard model. Most of the astroparticle questions can only be answered by multi wavelength observations. Thus CTA will make observations together with instruments covering the energy range from radio up to X-rays and low energy γ-rays.

The proposed Cherenkov Telescope Array (CTA) will consist of two arrays, a larger one

on the southern hemisphere and a smaller one on the northern hemisphere. Two arrays are needed to be able to observe the whole sky. The one on the southern hemisphere will observe the central region of our galaxy, where many sources with various morphologies can be found. Additionally extragalactic sources can be investigated. The northern array will be dedicated to study AGN as well as cosmological galaxy and star formation and evolution.

Three types of telescopes will be built and spread over a large area (some km^2): many small size telescopes (SST) of 6 m diameter, several middle size telescopes (MST) of 12 m diameter and some large size telescopes (LST) of 23 m diameter. The CTA consortium has not yet decided about the exact number of the different telescope types. The LSTs are needed to decrease the energy threshold below 100 GeV, while the SSTs will detect showers with energies above some TeV. Fig. 2.3 shows a photomontage of a possible CTA layout.

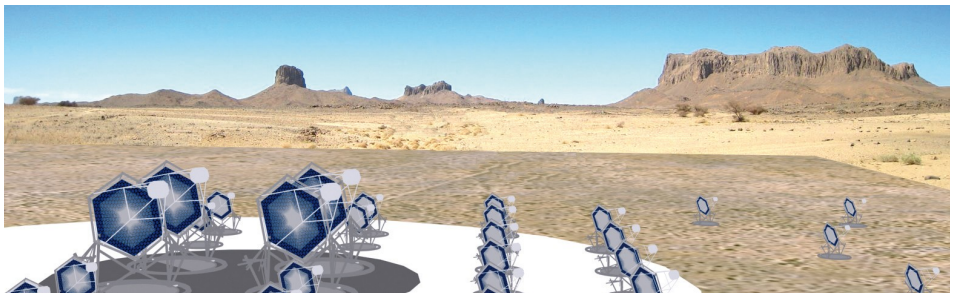

Figure 2.3.: Photomontage of a possible layout for CTA with few LSTs for the low energies, some MSTs, and many SSTs for the high energies. Picture from CTA Consortium (2010).

The performance goals CTA wants to achieve are the following (based on the CTA design report CTA Consortium, 2010):

Energy range The coverage of a large energy range is essential to understand most of the astronomical phenomena nowadays. The core energy range will be between 100 GeV and some TeV, the full energy range will be three to four orders of magnitude.

Sensitivity The improvement in sensitivity will be a factor of 10 compared to the best current telescopes. Therefore the number of sources will increase and allow deep population studies. New types of γ-ray emitters with lower intensities might be found and in the known classes weaker sources will be detected. The sensitivity in the core energy range will be milli-Crab (referring to the Crab Nebula as standard

candle). A simulation for the sensitivity of CTA can be seen in Fig. 2.4.

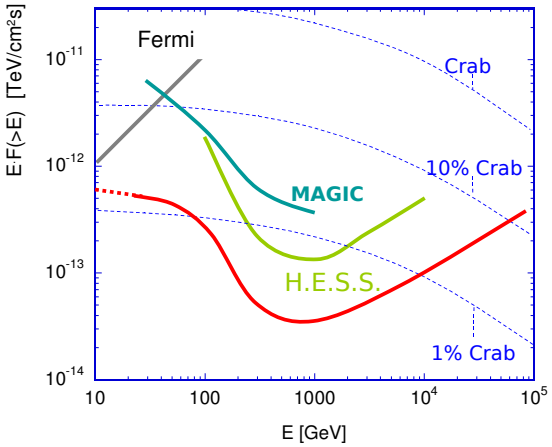

Figure 2.4.: Result for the sensitivity of CTA obtained by simulations in red compared to the sensitivities of current instruments; picture from CTA Consortium (2010).

Angular resolution CTA will surpass the current instruments by a factor of 5 in angular resolution, i.e. the angular resolution will be in the arc-minute range. This will make the study of the fine structures of sources, e.g., the shells of supernova remnants, possible.

Temporal resolution The large detection area of CTA will lead to a temporal resolution below one minute. At the moment phenomena (e.g. flares) varying at the few-minutes time scale have been detected. The possibility to observe periodic emission, e.g., from inner stable orbits around black holes, will arise.

Flexibility CTA will have different configurations: one extreme will be the observation of one object at full depth, the contrary extreme will be to observe different sources at the same time. In between those two many different configurations can be thought of. In addition it will be possible to do a full-sky survey at high sensitivity, where the telescopes are grouped and then observe the sky with overlapping fields of view.

Number of sources It is presumed that CTA will detect about 1000 γ-ray emitting objects, in the case that the currently known intensity distribution can be extended to lower energies.

Global coverage Building arrays on both hemispheres, CTA is planned to provide full

sky coverage. The tools to extract and analyse data will be the same.

In the last years the performance of Cherenkov telescope arrays has been studied in detail, demonstrating that the goals can be reached. The studies about the final layout are still ongoing, but a prototype for a middle size telescope will be built in 2011.

2.3. Mirror facets

For CTA the amount of mirrors to be produced is higher than for any existing IACT telescope. A replica technology would ease the mass production of mirror facets. The mirror facets have to be light-weight, robust and cost-effective with suited reflectivity and focussing quality. The focussing quality is described by the **point spread function (PSF)**, characterized here by d_{80}, the diameter containing 80% of the reflected light. For a one dimensional Gaussian d_{80} is $2 \cdot 1.29\,\sigma$ with the standard deviation σ; for a two dimensional Gaussian

$$d_{80}^{\text{length}} = 2 \cdot \sqrt{2 \cdot \ln 5}\,\sigma = 2 \cdot 1.79\,\sigma.$$

To compare mirrors with different focal length the value of d_{80} in mm (denoted with d_{80}^{length}) is not suited since it depends on the focal length. To overcome this, d_{80} is often expressed as the opening angle, denoted here with d_{80}^{angle}:

$$d_{80}^{\text{angle}} = \arctan \frac{d_{80}^{\text{length}}}{2 \cdot f} \approx \frac{d_{80}^{\text{length}}}{2 \cdot f} \tag{2.1}$$

We can approximate $\arctan x \approx x$ since the angles are small, usually below 1 mrad. The PSFs required for IACTs are not as small as for optical telescopes. The specifications for the MST mirrors are shown in Tab. 2.2. The mirror facets will have a hexagonal shape to

Table 2.2.: Baseline specifications for mirror facets for the MST, from CTA Consortium (2010).

Parameter	value
shape	hexagonal
size	1200 mm flat-to-flat
type	spherical
focal length	17 m (dep. on telescope design)
reflectance	$> 80\%$ between 300 and 600 nm
point spread function	< 1 mrad diameter (80% containment)

cover as much of the area as possible with only small spaces in between. To decrease the number of mirror facets per telescope the size will be 1.2 m flat-to-flat. The type of the mirror facets depends on the telescope design, for Davis-Cotton-designs spherical mirrors are used. The MST will have a Davis-Cotton-design and the mirror facets will have a spherical surface which is easy to produce. Whether the mirrors for the other telescope types will also be spherical or parabolic shaped is not decided yet. The focal length of the MST will be 17 m. The specification for the reflectance is $> 80\%$ between 300 and 600 nm to make sure that as many photons as possible get reflected. The reflected photons have to be focussed into a small spot, therefore the PSF has to be smaller than 1 mrad. For CTA different technologies to produce mirror facets with the required specifications are under investigation:

- glass mirrors
- diamond-milled aluminium mirrors
- cold slumped glas mirrors
- carbon-fibre composite mirrors

For the H.E.S.S., HEGRA and VERITAS telescopes **glass mirrors** are used, see Bernlöhr et al. (2003) and Cornils et al. (2003). The glass pieces (about 1 cm thick) are formed by machines, polished and then coated with a reflecting aluminium layer. Afterwards a layer of protecting material is added, in the case of the H.E.S.S. mirrors SiO_2 is used. This layer should make the mirror water and dust resistant. Since the telescopes have no shelter the mirrors are exposed to wind and weather the whole year. Even despite the coating, measurements show that the reflectivity is reduced by $\approx 5\%$ per year. Another issue is the weight of the mirrors, the H.E.S.S. mirror facets weigh ~ 10 kg and have a diameter of 60 cm. The advantages of the glass mirrors are the high reflectivity and the good point spread function. There is already a lot of experience with this technique.

The MAGIC telescopes have two different types of mirror facets which can be seen in Fig. 2.5. The **diamond-milled aluminium mirrors**, shown in Fig. 2.5(a) consist of an aluminium hexcell honeycomb structure with two aluminium layers (1 mm) on top and below. The three parts are glued together and form the so-called raw-blank. The raw-blank gets its final shape in two steps, first a rough pre-milling and second a high precision diamond-milling. The diamond-milling results in an average reflectivity of 85% and the required radius of curvature. A thin (100 nm) layer of quartz is added to prevent the mirror from corrosion and acid rain. The diamond-milled mirrors show a lower loss of reflectivity by cause of ageing but the achieved initial reflectivity is lower. The point spread function is small, meaning $d_{80\,\mathrm{mm}} = 5$ mm at 17 m (shown by Doro, 2010).

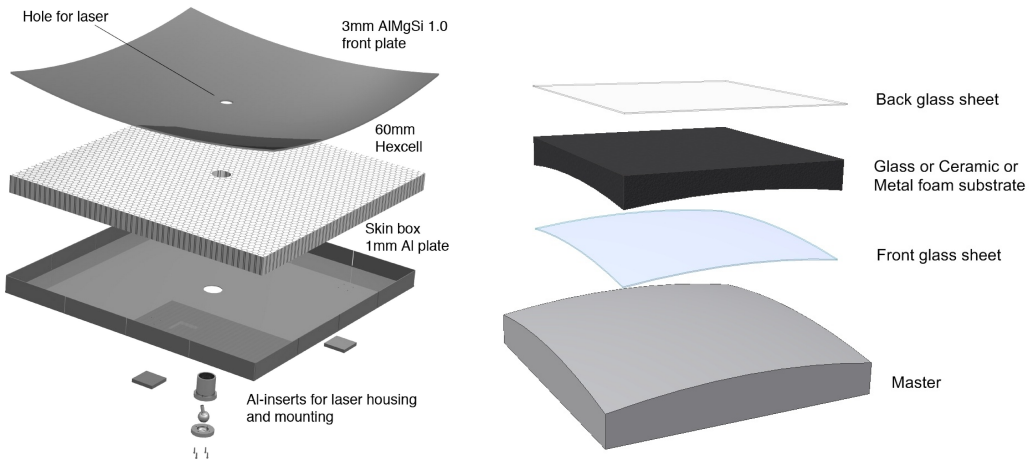

(a) Diamond-milled aluminium mirror (b) Cold slumped mirror

Figure 2.5.: Sketches of the two types of the MAGIC II mirrors, pictures from CTA Consortium (2010).

The production of **cold slumped glass mirrors**, which are shown in Fig. 2.5(b), is done with a high quality mold, which has the requested radius of curvature. The thin glass layer (1 – 2 mm) is pressed against the mold using a suction system. The core material and the second layer of glass are glued to it. Afterwards the front glass layer is coated with aluminium and a quartz layer for protection. As a core material a honeycomb hexcell structure was used for half of the MAGIC II mirrors. At the moment different materials are tested for CTA, among others foam. The MAGIC II mirrors have an average reflectivity of 90% and a point spread function smaller than 2 mrad.

One type of **Carbon-fibre composite mirrors** is developed by the CTA working group in Saclay (as presented by Brun, 2010). Their approach is to use preshaped strips made of carbon or aluminium for the support structure and a mold with the requested radius of curvature. The stripes are glued together resulting in a stiff support structure with the same radius of curvature. A carbon layer (thickness 1.5 mm) is placed on the mold which has a suction system. On this mold the carbon layer is glued to the support structure, in this way the carbon layer is sandwiched between the two parts with the requested radius. Another layer of carbon is glued to the backside of the mirror. After 12 hours of polymerization a borofloat glass layer (1.1 mm thick) is glued to the curved carbon layer (see Figure 2.6).

For CTA the decision which mirrors will be put on the telescopes is not made yet. This thesis aims to give valid input to that question. At the moment there are groups at

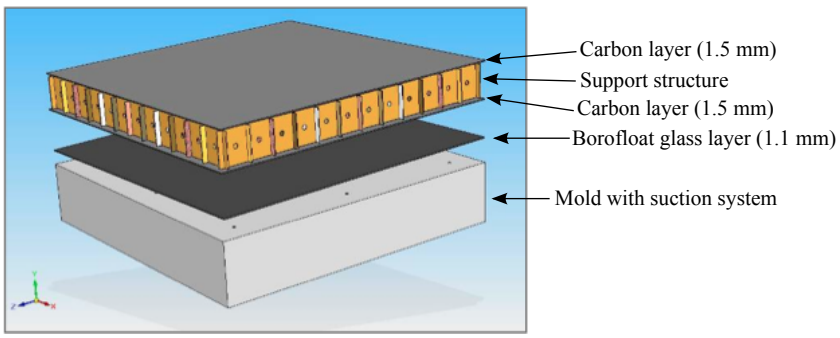

Figure 2.6.: Sketch of the different layers of the mirror facets produced in Saclay, picture from CTA Consortium (2010).

different universities working on the production of mirror facet prototypes. The only technique which is until now used to characterize mirror facets is the $2f$ method which will be described in the following chapter. With this method only the PSF and the focal length of the mirrors can be measured. But especially during the development phase it is very helpful to get information about the surface quality of the mirror facets.

The result of the $2f$ measurement is only a datum for d_{80}, but with a surface measurement it is possible to give detailed information about the underlying structure. If, for example, the inner part of the mirror facet has the required shape but the outer parts do not fulfil the requirements this information can be given back to the manufacturers. Another problem that might occur using a honeycomb structure is that the structure of the honeycomb might be transferred to the reflecting surface. This can also be directly checked with a surface measurement.

Another crucial property is the change of the mirror facet's surface with temperature. The mirror facets have to be resistant to temperature changes between -10 and $+40°$ C, a typical temperature range for the sites which are evaluated. In the large $2f$ setting this temperature range can not be covered in the lab.

A successful method to measure specular surfaces is Phase Measuring Deflectometry (PMD). PMD was developed at the institute of optics at our university. It is mainly used to check the quality of progressive eyeglass lenses, but also to measure windscreens of cars. The main topic of this thesis is the applicability of the PMD method to IACT mirror facets. To confirm that this metrology is well-suited for this purpose, we compared the results of the PMD with the ones from the $2f$ measurement. In the framework of the thesis we tested different prototypes of mirror facets and a standard H.E.S.S. facet, a summary is shown in Tab. 2.3.

Table 2.3.: Mirror prototypes which have been tested, † size denotes the diameter for round mirrors and the edge length for quadratic ones.

Name	Place of production	Core material	Shape	Size † [cm]	Focal length nominal,[m]
H.E.S.S. A 153	Armenia	glass	round	60	30
small H.E.S.S. test 1194	Czech Republic	glass	round	30	1.194
small H.E.S.S. test 641	Czech Republic	glass	round	30	0.641
Saclay aluminium	Saclay	aluminium	quadratic	50	30
Saclay carbon	Saclay	carbon	quadratic	50	30
Cracow glass	Cracow	aluminium	round	30	30
Cracow epoxy	Cracow	aluminium	round	30	30

3. Measurement at $2f$

As the quality of the mirror facets has to be checked before they are mounted onto the telescope, a test setup was developed. The first setup was designed at the University of Heidelberg and the Max-Planck-Institute for Nuclear Physics in Heidelberg (MPIK) to measure the characteristics of mirror facets for the H.E.S.S. telescopes. Three master theses were written on this topic, see Elfahem (1999); Schreiber (2005); Giavitto (2007). We reconstructed the original setup at our institute to utilize it for CTA mirror measurements. The new setup had new systematics, which we examined. We measured different prototype mirror facets for CTA and three H.E.S.S. mirror facets.

3.1. Principle of measurement

The Heidelberg setup is a so-called $2f$ setup. The object (the light source) and the image are at a distance of twice the focal length (f) from the mirror. You can use the mirror formula

$$\frac{1}{b} + \frac{1}{g} = \frac{1}{f} \tag{3.1}$$

where b is the distance of the image from the mirror and g is the distance of the object from the mirror to calculate the following: if you put a point-like light source at a distance of $g = 2 \cdot f$ the image can be seen in the same distance, as the incoming rays hit the surface of the mirror perpendicularly and are reflected back in the incoming direction, assuming spherical mirrors.

This is the smallest optical imaging setup to check the imaging quality of the mirror

properly. The only possibility to get a setup with a shorter length, would be to produce parallel light rays which hit the surface and get focussed at a distance of f from the mirror. The problem with the one f setup is that one needs a light source emitting parallel rays which illuminate the whole mirror facet, which is much harder to realize.

The equipment needed to build a $2f$ setup is: a light source, a detector to measure the picture of the light source which is produced by the investigated mirror facet and a dark room which is large enough. A sketch of the $2f$ setup can be seen in Fig. 3.1.

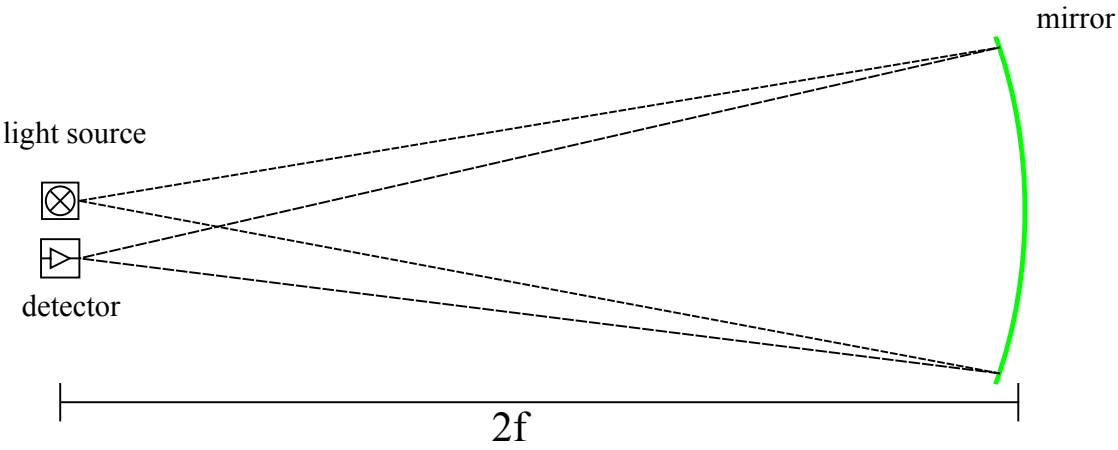

Figure 3.1.: Sketch of the $2f$ measurement setup. The distance between the light source and the detector is shown extremely increased to demonstrate the light rays more clearly.

3.2. Setup

To measure the point spread function of a mirror facet we put a light source at a distance of $2f$ from the mirror facet and detect the reflected picture of the light source at the same distance. We tested different light sources: lasers at different wavelengths with additional optical lenses to widen the beam and a light emitting diode (LED).

As detectors we compared different photodiodes and a CCD Camera (Adimec 1000m). In the diode-measurements a reversed-biasing voltage is applied to the diode and the incoming light leads to a current which is measured by an ampere meter. The sensitive area of the photodiode is rather small and the photodiode is not imaging. Not imaging means that it detects only the amount of light hitting the whole sensitive area, it is not

possible to find out which part of the sensitive area is exposed to the light. Therefore we use a setup with stepping motors to move the diode in the x- and y-direction. The stepping motors have a minimal stepsize of $s = 6.25\,\mu$m and are controlled by a computer. The area which can be scanned with our setup is $20 \times 30\,$cm, this is large enough to also measure mirrors with a large PSF.

We mainly utilized two different photodiodes, the first one is a Siemens Osram SFH 206 K which has a sensitive area of $2.65 \times 2.65\,\text{mm} = 7\,\text{mm}^2$. It is suitable for applications from $400 - 1100\,$nm and has a short switching time of $20\,$ns. For technical details see Siemens AG (1998). The second one is a Siemens Osram SFH 309 with a small sensitive area of $0.2\,\text{mm}^2$ and a high linearity. The dark current is very low ($<1\,$nA), while the fall time is smaller than $10\,\mu$s. All technical details can be found in Siemens AG (1997).

Alternatively we used a CCD camera, we choose the Adimec 1000m, which has 1 Megapixel and a pixel-size of $7.4 \times 7.4\,\mu$m. It has the advantage of a much faster measurement, but the disadvantage that the area which can be detected is only $7.4 \times 7.4\,$mm and the dynamic range is limited. Due to the small area only very good mirror facets can be tested. To analyze larger PSFs a lens would be needed which requires an additional calibration and by itself distorts the picture.

3.3. Systematic studies

We carried out different studies on our setup to understand systematic effects. To perform a measurement it is necessary that the background light is as small as possible. If the PSF is measured at daylight the background light would be too bright. Therefore we realized a $2f$ setup in the cellar of our institute, see Fig. 3.2, where a $30\,$m dark corridor was available.

In Fig. 3.2 the photodiode and the stepping motors which move the photodiode are clearly seen. The light source in the picture is the green laser, the additional lens to widen the beam cannot be seen. We tested the temporal stability of the light sources: after a 10 minutes warming phase the variations are smaller than 0.5%.

The measured values, the current in the case of the diode and the pixel-values in the case of the camera, are filled into a histogram. To find out the background value, the light source is switched off and an equivalent measurement is done. This background value is then subtracted in each bin separately.

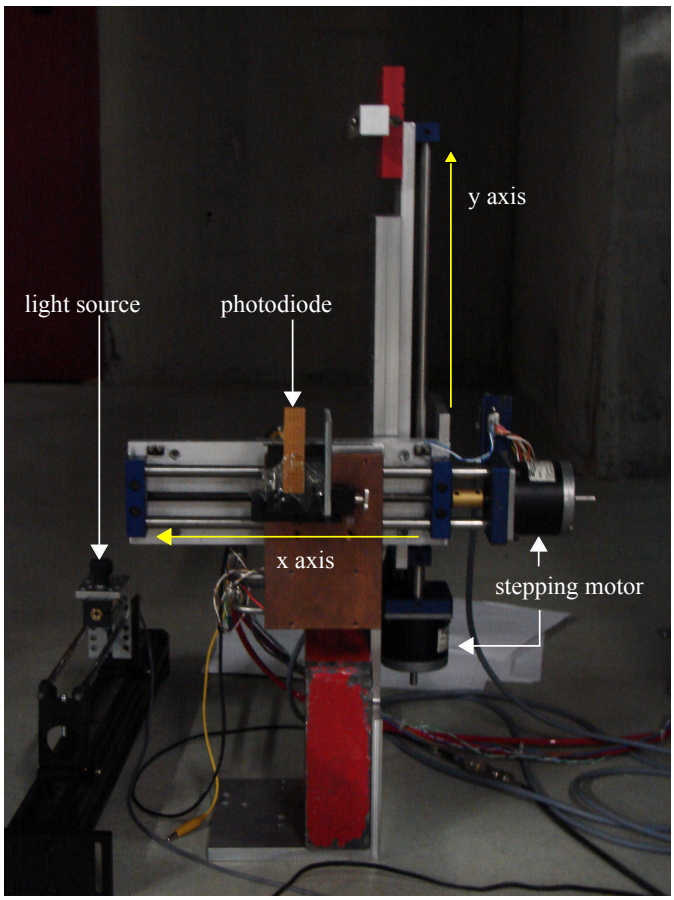

Figure 3.2.: The $2f$ measurement setup in the cellar of the institute.

3.3.1. Light sources

The light source is an important part of the setup. It is necessary that the light covers the whole mirror uniformly in a distance of $2f$. If the light source itself has some structure it is hard to find out about the PSF of the mirror facet, since the resulting picture will be a convolution of the structure of the light source and the PSF of the mirror facet. In the case of the lasers we use a lens to widen the beam, otherwise the laser would hit only a part of the mirror and then only the PSF for this part would be measured. These results would not be practical for a comparison of the PSFs obtained with different techniques. However, the lens imprints its structure on the light beam and has consequently to be taken into account additionally.

Table 3.1.: Comparison of the fitted σ-values of the Saclay aluminium mirror for different light sources using the diode 206 as light detector.

Light source	LED	Red laser	Green laser
σ_x [mm]	17.09 ± 0.24	18.91 ± 0.11	18.49 ± 0.15
σ_y [mm]	19.87 ± 0.26	22.97 ± 0.15	23.06 ± 0.20

We compare three different light sources: a LED, a green laser, and a red laser and judge their usability by comparing the resulting d_{80}-values of the Saclay aluminium mirror facet. We use diode 206 as light detector, the results are shown in Fig. 3.3.

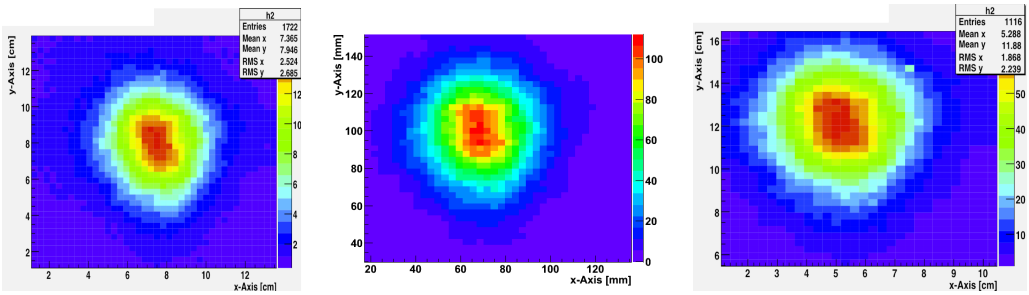

(a) LED (b) Red laser with lens (c) Green laser with lens

Figure 3.3.: PSF of the Saclay aluminium mirror for different light sources, in all the background was subtracted. Note that the axes are not the same for the three pictures.

The total amount of light is calculated by adding up the values in the whole histogram after subtracting the background. We did a background measurement and subtracted the mean value in each measurement point.

To calculate d_{80} we projected the histograms on the respective axis and fitted a Gaussian to the projections. The results, shown in Tab. 3.1 are promising, the size is about the same for all three light sources and no substructure is recognizable. The σ-values for the diode are slightly smaller than for the lasers, this leads to the assumption that the light emitting area of the LED is smaller. To get information about the overall size and shape of the PSF the lasers are also suited, but for the study of detailed features the diode is better. The only drawback of the LED is the lower intensity. If it is necessary to measure mirrors which have a bad reflectivity and / or a large PSF, the intensity of the reflected light will be too low to measure it with the photodiode because of its dark current.

The quality of the light sources was also inspected by looking at the structure of the light spot in some distance. At a distance of $2f$ the structure of the light source becomes

Table 3.2.: Comparison of the σ values for different rotation angles Θ, σ_x and σ_y are the values in the rotated coordinate system.

Θ	0°	90°	180°	270°
σ_x [mm]	16.92 ± 0.14	16.12 ± 0.15	16.76 ± 0.18	16.13 ± 0.30
σ_y [mm]	20.98 ± 0.27	21.02 ± 0.20	20.04 ± 0.16	21.45 ± 0.27

better visible because the light is spread over a larger area. One can see with the eye that the diode has a higher uniformity than the lasers with the lenses. This is confirmed by the calculations of the σ-values.

Rotation of the mirror

To investigate whether the measured structure is determined by the mirror facet and not the light source we did the following check: we measured the PSF as described above and marked the position of the mirror facet. We rotated the mirror facet and measured the PSF at different rotation angles Θ. The results shown in Fig. 3.4 and Tab. 3.2 are obtained with the aluminium mirror from Saclay and the red laser as light source.

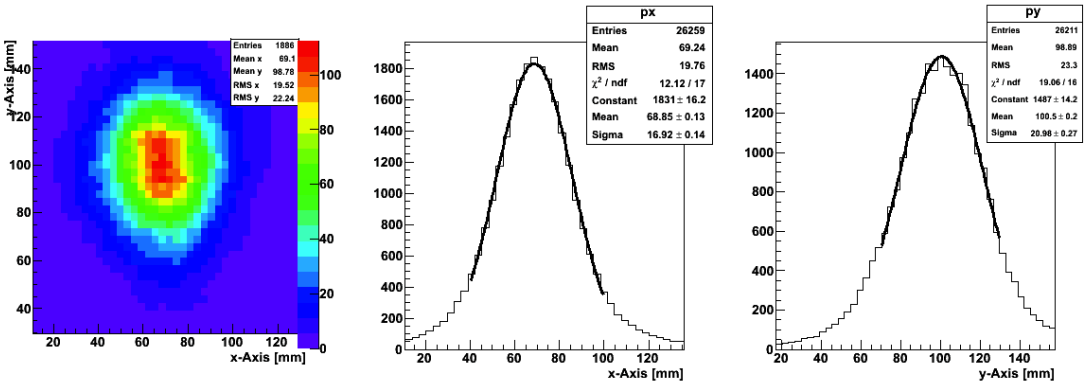

Figure 3.4.: The PSF measurement of the aluminium mirror from Saclay.

We performed a fit of a Gaussian to the one dimensional projections. Tab. 3.2 shows the different results for the fits, where σ is the width of the Gaussian. The axes of the mirror are taken to be the same for all measurements, we rotate the coordinate system accordingly.

The results show that the structure we see really belongs to the mirror as it rotates together with the mirror. But the values for σ_x and σ_y show a hint of a small systematic error, the values are not completely compatible within their respective statistical errors. Fig. 3.5 shows the σ_x- and σ_y-values for the different rotation angles Θ for the aluminium mirror from Saclay.

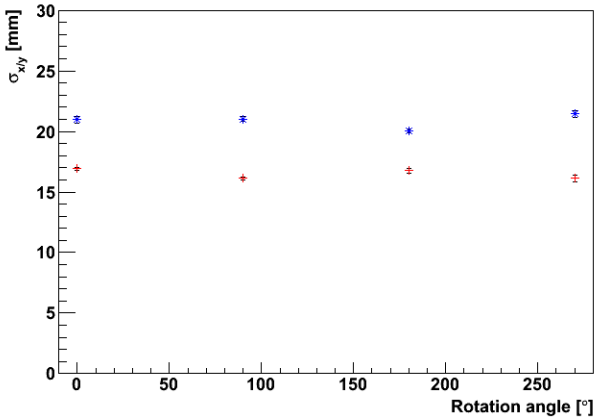

Figure 3.5.: The σ_x- and σ_y-values for the different rotation angles Θ for the aluminium mirror from Saclay. The red crosses denote the values for σ_x and the blue stars denote the values for σ_y.

Light sources for mirrors with very small PSFs

To investigate the light sources we also analysed the PSF of the H.E.S.S. A153 mirror facet, the results are shown in Fig. 3.6 and Tab. 3.3. We used the photodiode 309 as detector, since it has a short edge length and therefore resolves all features, further investigations for the light detection are shown in the next paragraph. The size of the point spread function is about the same for all three light sources, but the PSFs show different characteristics. The LED-PSF is the smallest of the three, this leads to the assumption that the laser beams widened by the lenses have a larger light emitting area, i.e., they are less point-like. While the laser-PSFs show a hole in the middle part of the PSF the LED-PSF has no such feature. The hole structure may come from the lenses used to widen the laser beams.

Since the point spread functions (see Fig. 3.6) are not symmetric in x and y we project the histograms on the respective axis. We calculated the size of the interval containing 80% of the reflected light (d_{80}) for both projections in the following way. We assigned

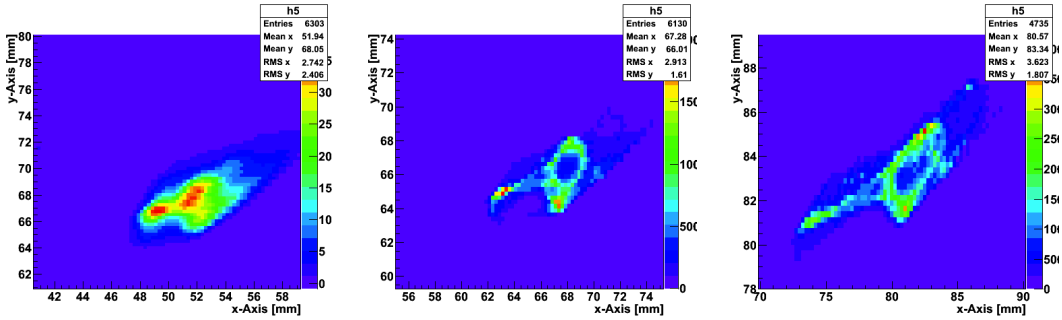

(a) LED (b) Red laser with lens (c) Green laser with lens

Figure 3.6.: Comparison of different light sources, in all the background was subtracted.

Table 3.3.: Comparison of d_{80} for different light sources.

Light source	LED	Red laser	Green laser
d_{80} projection on x axis [mm]	5.5	8.0	10.0
d_{80} projection on y axis [mm]	4.0	4.0	4.5

the center of the interval to be the mean value and enlarged the interval until 80% of the total amount of light was reached. The results of the d_{80} calculations are shown in Tab. 3.3.

These measurements show that for the detailed investigation of very small PSFs the LED is the best choice. The lasers with the lenses have a larger structure than the diode and should only be used for mirrors with a larger PSF than the H.E.S.S. A153 mirror.

3.3.2. Light detection

Another important question is how the light detection technique influences the measured values. Therefore different detection techniques are compared. The stepping motors have a step size of 6.25 μm. Compared to both, the area of the photodiode and the PSF this is really small, making it unnecessary to sample the image at every single step of the motor. Instead we choose a step range of 40 to 100 steps, depending on the required spatial resolution.

The investigation of the different light sources was done with the H.E.S.S. mirror A153 using the LED as light source. The first measurement is done with the small diode 309

Table 3.4.: Comparison of d_{80} for different detectors, using the diode as light source. The statistical errors for these fits are in the order of 0.05 or below. The systematic errors will be clarified in further measurements.

Detector	Diode 206	Diode 309 convolved	Diode 309	Adimec
d_{80} x axis [mm]	5.38	5.92	4.21	4.25
d_{80} y axis [mm]	4.76	4.45	3.51	3.58

and a step range of 40 steps, see Fig. 3.7(a). This means we have data points every $40 \cdot 6.25\,\mu\text{m} = 250\,\mu\text{m}$. The measurement of the whole area takes about two hours.

The next measurement is done with the larger diode 206 and a step range of 100 steps ($625\,\mu\text{m}$), the edge length of the diode is 2.65 mm. In this case the spot is oversampled, which can be seen in Fig. 3.7(b). To compare the measurements we convolved the 309-measurement with a function equal to the area of diode 206, see Fig. 3.7(c).

The last measurement is done with the CCD camera, see Fig. 3.7(d). The large difference regarding d_{80} between the diodes (especially the large diode 206) and the CCD camera is not surprising, since the camera has a pixel-size of $7.4\,\mu\text{m}$ which is much smaller than the edge length of 2.65 mm. The larger edge length leads to a larger PSF for the following reason: the diode detects the light spot as soon as one part of the diode is illuminated, it might be the case that the edge of the illuminated area is only 1 mm, but this cannot be resolved by the measurement of the photo current. This effect can nicely be seen in Fig. 3.7, the only difference between Fig. a) and c) is the convolution with a square with an edge length of 2.65 mm.

We did projections on the axes and calculated d_{80} based on a Gaussian fit. The results are shown in Tab. 3.4.

Looking at Tab. 3.4 and Fig. 3.7 the best detectors are the diode 309 and the camera. Diode 206 has a too large edge length to scan the PSF in detail, but the overall shape is the same as with diode 309.

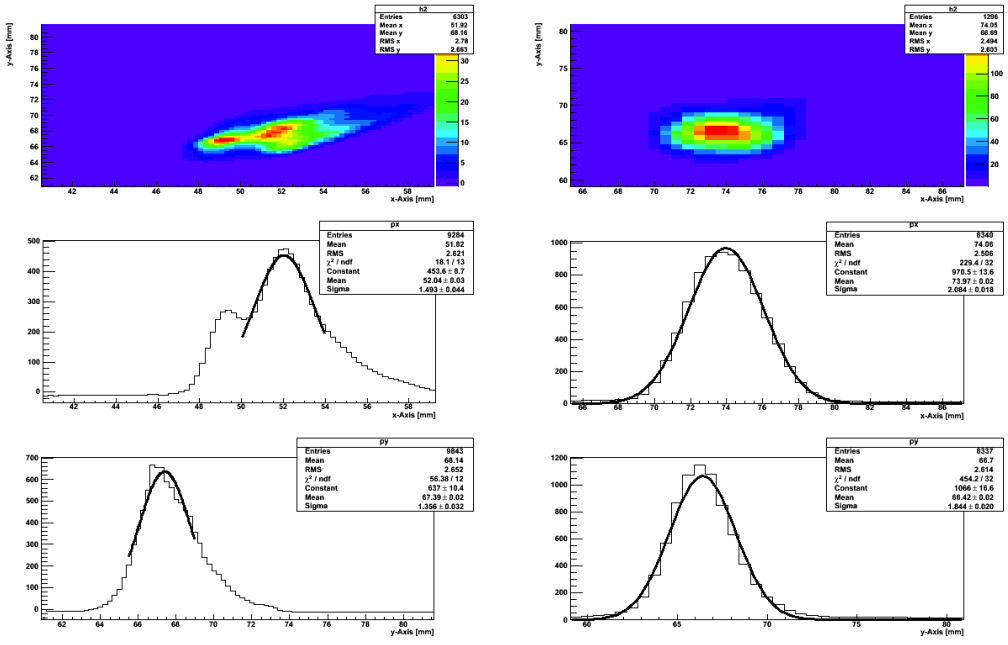

(a) Diode 309 step 40

(b) Diode 206 step 100

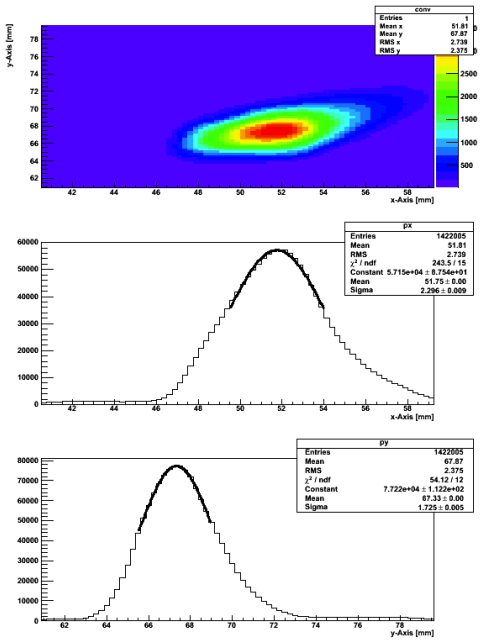

(c) Convolution diode 309 step 40

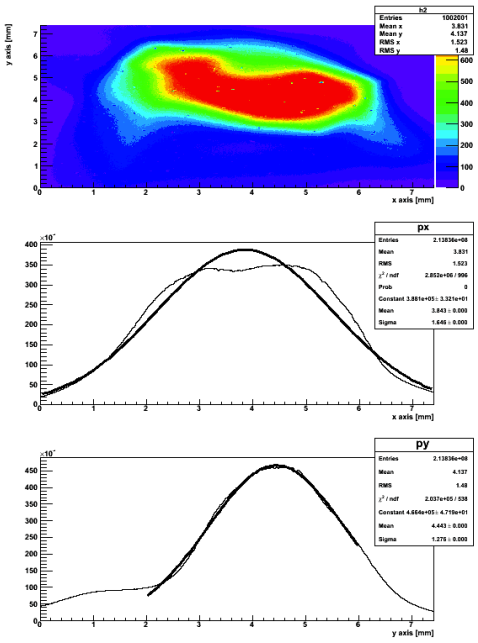

(d) Adimec

Figure 3.7.: Comparison of different detectors. Note that the axes for the Adimec camera are not the same as for the other measurements.

3.4. Focal length measurements

The $2f$ setup also includes the possibility to measure the focal length of mirror facets directly. Several pictures of the PSF were taken at different distances from the mirror facet. The focal length is determined by the minimum size of the PSF. Knowing the distance of the image with the smallest PSF to the mirror (b) and the distance of the object to the mirror (g) we can use the mirror formula (equation 3.1) to calculate the focal length (f) of the mirror.
An example for a focal length measurement is shown in Fig. 3.8, where five measurements were done at different distances b from the mirror. We used the small H.E.S.S. mirror 1194, the diode as light source and the Adimec camera as detector.

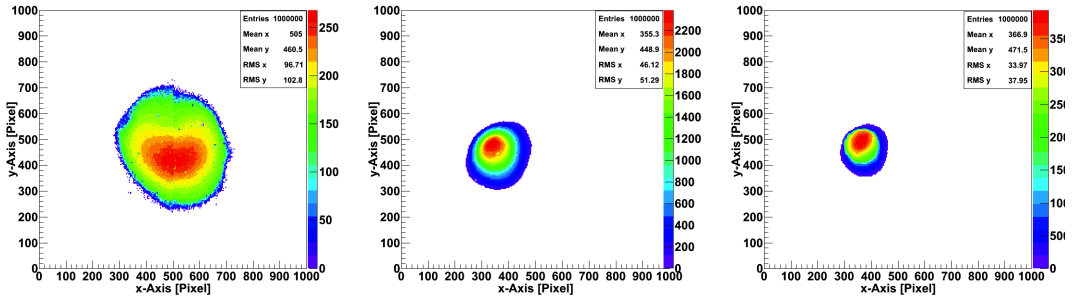

(a) $b = 55\,\text{cm}$

(b) $b = 58\,\text{cm}$

(c) $b = 60\,\text{cm}$

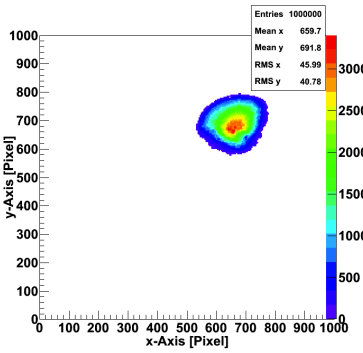

(d) $b = 62\,\text{cm}$

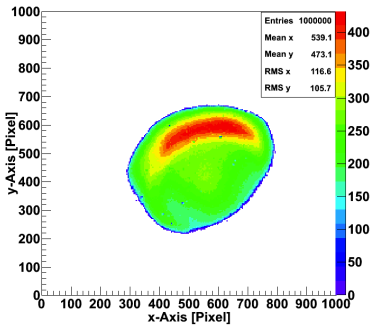

(e) $b = 65\,\text{cm}$

Figure 3.8.: PSFs at different distances b from the mirror.

By fitting a Gaussian function to the projections we obtained the values for the widths σ_x and σ_y. The area A of the spot is proportional to $\sigma_x \times \sigma_y$. To find the minimum PSF

we fitted a parabola to the values for the area of the PSF in dependence of the distance. The fit result is shown in Fig. 3.9, with a minimum value at $b = 59.92 \pm 0.19\,\text{cm}$.

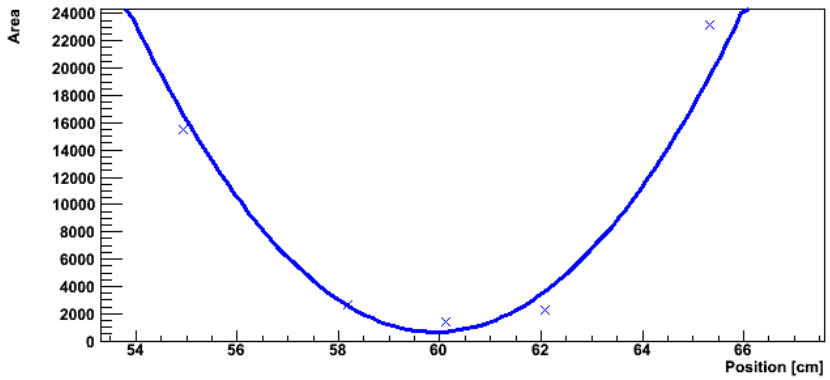

Figure 3.9.: Fit result for the parabola fit to the area of the spot for mirror H.E.S.S. test 1194.

Knowing that the distance of the light source from the mirror is $g = 232\,\text{cm}$, we calculated the focal length to be 118.2 cm. This is close to the value obtained by a measurement in Heidelberg, which is 119.4 cm.

The focal length is an important specification of a mirror, but after the mirror facets are mounted onto the telescope only the size of the PSF in the nominal focal length is critical. Whether the PSF of a mirror facet is smaller at a distance which is not the nominal focal distance does not change the imaging behaviour. Therefore focal length measurements were only done for the three H.E.S.S. mirrors.

3.5. $2f$ measurements for different mirror facets

In this section the results for the different mirror facets are summarized. The requirement for the mirror facets is to have a PSF, here denoted with d_{80}^{angle}, smaller than 1 mrad, as can be seen in Tab. 2.2. If not stated otherwise the LED and diode 309 were used as light source and detector.

Table 3.5.: The characteristic values obtained by the $2f$ measurement for the H.E.S.S. A153 mirror.

Direction	σ [mm]	d_{80}^{length} [mm]	d_{80}^{angle} [mrad]
x-direction	1.63	4.21	0.14
y-direction	1.36	3.51	0.12

Table 3.6.: The characteristic values obtained by the $2f$ measurement for the small H.E.S.S. 1194 and 641 test mirror.

Direction	Mirror 1194			Mirror 641		
	σ [mm]	d_{80}^{length} [mm]	d_{80}^{angle} [mrad]	σ [mm]	d_{80}^{length} [mm]	d_{80}^{angle} [mrad]
x-direction	0.28	0.73	0.31	0.26	0.67	0.54
y-direction	0.27	0.69	0.29	0.40	1.03	0.80

H.E.S.S. A153 mirror

Some results of the H.E.S.S. A153 mirror were already shown in Sects. 3.3.1 and 3.3.2. After fitting a Gaussian to the projections, we used the parameters to determine d_{80}, the results are shown in Tab. 3.5.

The PSF of the H.E.S.S. A153 mirror is in all cases smaller than 0.2 mrad. Therefore the requirement for CTA would be fulfilled by the H.E.S.S. mirror facets. The H.E.S.S. mirrors will, however, not be used for CTA due to their high weight and high costs.

H.E.S.S. 1194

The results for the H.E.S.S. 1194 test mirror were already presented in Sect. 3.4.

This mirror has an extreme small PSF, as shown in Tab. 3.6, and would also fulfil the specifications for CTA.

H.E.S.S. 641

The measurements done with the H.E.S.S. 1194 mirror have also been carried out with the H.E.S.S. 641 mirror. The calculations led to a focal length of 64.2 cm, which is very close to the value of 64.1 cm, as measured in Heidelberg. The PSF at this distance can be seen in Fig. 3.10. By fitting a Gaussian to the projections one obtains values for σ_x and σ_y, the results are shown in Tab. 3.6.

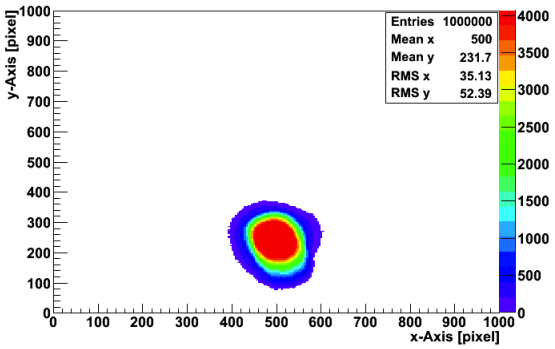

Figure 3.10.: PSF of the H.E.S.S. 641 mirror, using the diode as light source and the Adimec camera as detector.

This mirror also shows a small PSF, however not as good as the other small H.E.S.S. mirror, but still fulfilling the specifications for CTA. Although one has to keep in mind that the small H.E.S.S. test mirrors have not the specified focal length.

Saclay aluminium mirror

Using the results from Sect. 3.3.1 "Rotation of the mirror", the four measurements were used to obtained a mean value for d_{80}. The results are shown in Tab. 3.7.

The aluminium mirror facet is a real prototype from Saclay for the middle size telescope and does not completely fulfil the requirements concerning the PSF for CTA as described in Tab. 2.2. This result is promising, but the technology needs to be further improved and the size of the mirror facets has to be increased to 1.2 m.

Table 3.7.: The characteristic values obtained by the $2f$ measurement for the Saclay aluminium mirror.

Direction	σ [mm]	d_{80}^{length} [mm]	d_{80}^{angle} [mrad]
x-direction	16.5	42.5	1.41
y-direction	20.9	53.8	1.79

Table 3.8.: The characteristic values obtained by the $2f$ measurement for the Cracow mirrors.

Direction	Epoxy mirror			Glass mirror		
	σ [mm]	d_{80}^{length} [mm]	d_{80}^{angle} [mrad]	σ [mm]	d_{80}^{length} [mm]	d_{80}^{angle} [mrad]
x-direction	18.5	47.6	1.59	20.4	52.6	1.75
y-direction	13.9	35.8	1.19	24.0	61.9	1.06

Saclay carbon mirror

The $2f$ measurement of the Saclay carbon mirror was done by Clementina Medina in Saclay. Her results of the carbon mirror are used for the comparison with the PMD results, shown in Chapter 5, but are not outlined here.

Cracow glass and epoxy

The mirror facet prototypes from Cracow were also tested with the $2f$ setup. The PSFs of the Cracow mirrors are larger than the other tested mirrors. It was not possible to use the diode as light source because the PSFs were large and the reflectivity low, therefore the spot was to weak to measure it.

To measure the epoxy as well as the glass mirror, we used the red laser as light source and the diode 206 as detector. We obtained the results shown in Fig. 3.11 and summarized in Tab. 3.8.

In the lower panels of Fig. 3.11 photographs of the light spots taken with a digital camera are shown. The pictures taken with the digital camera show more details in the structure which cannot be resolved by the scanning diode but the shape and the size are the same.

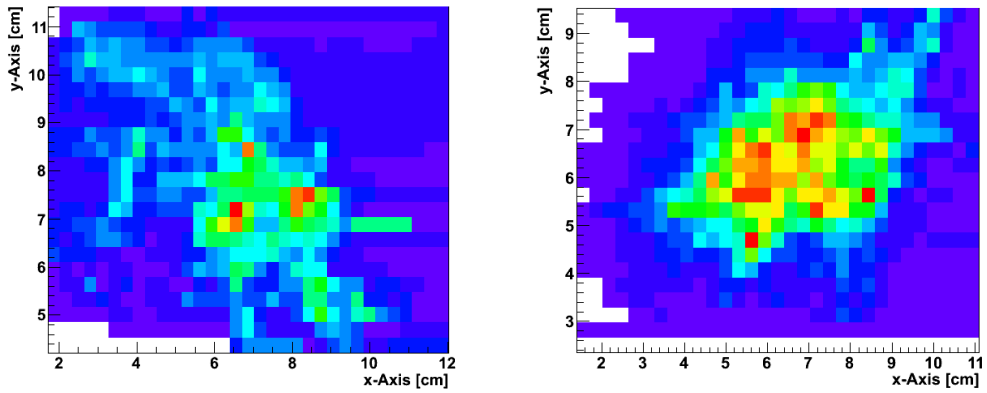

(a) Scan, glass mirror

(b) Scan, epoxy mirror

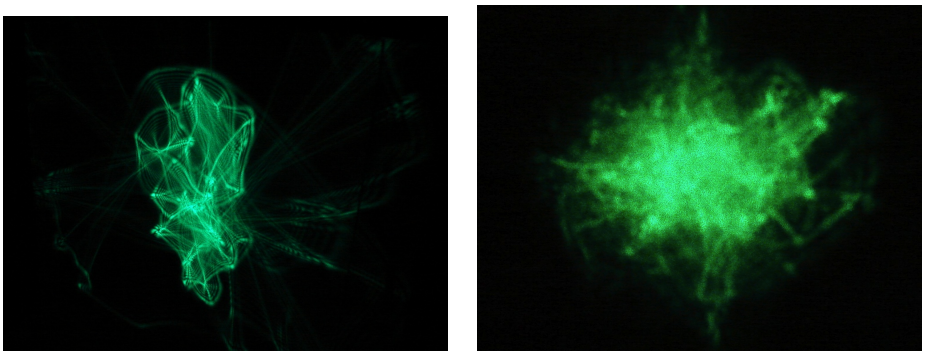

(c) Digital camera, glass mirror

(d) Digital camera, epoxy mirror

Figure 3.11.: PSF of the Cracow mirrors. In the upper panels the PSF when using the red laser as light source and a scanning diode is shown. The pictures shown in the lower panels are taken with a digital camera and the green laser as light source. The height of both pictures is $\approx 10\,\mathrm{cm}$.

The Cracow mirrors are also real prototypes for the middle size telescope for CTA, but they do not yet fulfil the specifications, the fabrication technology has to be improved slightly.

These results show the the $2f$ setup works fine, we did systematic studies on the light source and light detection technique and realized an optimized setup. We will further investigate the systematics, but this is beyond the scope of this thesis. We were able to provide valuable feedback to the groups in Saclay and Cracow about the characteristics of their mirrors.

4. Phase Measuring Deflectometry (PMD)

Phase Measuring Deflectometry (PMD) is a metrology to measure specular surfaces. It has been developed by the OSMIN group at the University of Erlangen[1]. The PMD is, among others, used to check the quality of progressive eyeglass lenses, windscreens and painted car bodies. A very sucessful project is the eyeglass measuring, a prototype setup to measure eyglass lenses was developed and is now in use in several eyeglass manufacturing companies.

In this chapter we will start with a general description of the measuring technique, followed by the characteristics of the mirrors one can measure with this method. To get a value for the PSF it is necessary to perform raytracing on the PMD-data which will be described. In the last section measurements and the results of several mirror facet prototypes, listed in Tab. 2.3, are shown.

4.1. Principle of measurement and systematics

This section is mainly following the description of Knauer (2006). The basic idea of PMD is to observe the distortions of a defined pattern after it has been reflected by the examined surface (see Fig. 4.1). From the distortions one can calculate the exact shape of the surface.

Reflection mainly depends on the normal of the surface, that is the reason why the slope of the object is the first measurand in deflectometric systems. Since specular surfaces reflect light monodirectionally, one has to make sure that the reflected rays hit the camera, i.e., the light source has to cover a large solid angle. One way to solve this is to use a big

[1] http://www.optik.uni-erlangen.de/osmin/

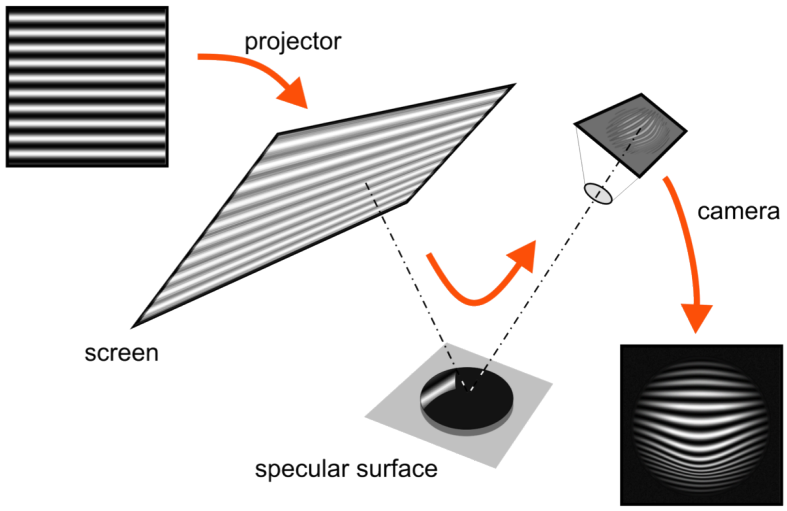

Figure 4.1.: Sketch of the measurement principle of PMD. The sinusoidal pattern is projected on a screen or a ground glass. The camera takes pictures of the distortions of the pattern due to the reflection on the object; picture from Knauer (2006)

screen, which is diffusely emitting. An important part of the technique is to code the position x on the screen by the projected pattern. PMD uses a sinusoidal pattern, which has the huge advantage that the phase of the sinus does not change even if the pattern is observed out of focus. It is not possible to observe the object and the pattern in focus at the same time. In order to conceive a high lateral resolution we focus on the object and defocus on the pattern. The only remaining problem is that the contrast decreases if we observe out of focus. Therefore the lateral and angular resolution (δx and $\delta\alpha$) are coupled and a limit for the conceivable accuracy can be determined, the detailed calculations are shown in the dissertation of Knauer (2006). Using the sinusoidal pattern it is possible to determine the phase in each pixel of the camera independently. To determine the phase known phase shift techniques like the Bruning four-shift-technique are used, in which four sinusoidal patterns with phase shifts of $\pi/2$ are projected onto the screen. To calculate the relation between the tilt of the surface and the phase we use the following (see Fig. 4.2):

$$\tan 2\alpha = \frac{x}{d} \qquad x = \varphi \cdot \frac{p}{2\pi} \qquad \Rightarrow \varphi = \frac{2\pi}{p} \cdot d \cdot \tan 2\alpha \tag{4.1}$$

But with only one slope one can not determine the position of the object in a three dimensional space, one needs the slope in two directions which are perpendicular to each other. Therefore the sinusoidal pattern is used two times, the first time horizontally,

leading to the slope in the x-direction and the second time vertically to find the values for the slope in y-direction. The calculations are obviously the same when replacing x with y in Eq. 4.1.

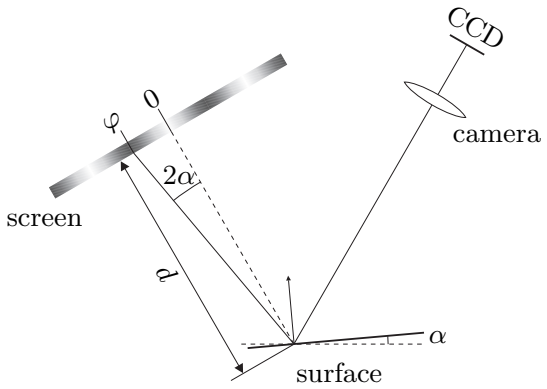

Figure 4.2.: Sketch of the rays in PMD, the phase φ corresponds to the tilt α with a know distance d and the period p of the sine, picture from Knauer (2006).

An open point is then the determination of the absolute height and therefore the normal of the surface. Although, after the calibration (described in the next paragraph), we know the line of sight of the camera ($\mathbf{v}$) and the position on the screen ($\mathbf{q}$), there are different normals fulfilling the criteria. The problem with two possible normals and according heights is shown in Fig. 4.3. You can see that the normal tilts in the plane which is defined by the position of the camera, the spot on the screen and the point on the surface where the ray is reflected if the height is changed.

Stereo deflectometry

One solution to solve the problem of the absolute measurement is to use a second camera and a stereo approach. The cameras have to be positioned with a large angle (close to 90°) between them. The normal always lays in the plane which is defined by the position of the camera, the spot on the screen and the point on the surface where the ray is reflected. If the height of the object is changed the normal tilts, but stays in the plane.

In Fig. 4.4 the optimal setup is shown. The cameras are at a large angle and the normal has only one direction which lays in both camera planes (E_1 and E_2). The intersection line of the camera planes is the only possible direction of the true normal.

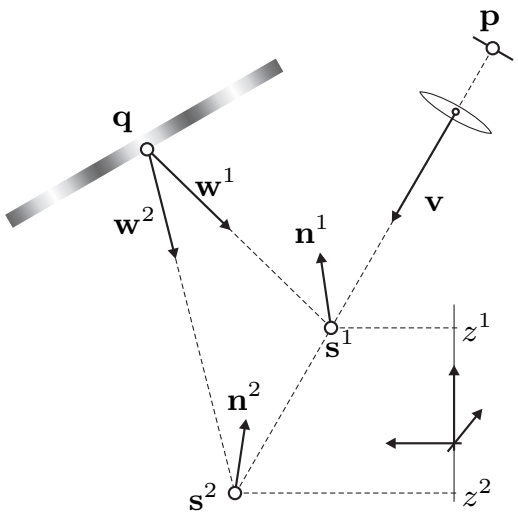

Figure 4.3.: Sketch showing the problem of the absolute measurement. Although **v** and **q** are known, different heights and normals are possible, in this sketch two possible heights (**s**) and normals (**n**) are shown; picture from Knauer (2006).

Calibration

All parts of the setup have to be calibrated and the different coordinates have to be translated into a common coordiante system, the so-called world coordinate system. Therefore the calibration is divided into three parts, the calibration of the projector, of the camera, and of the geometry. The calibration of the projector correlates the measured phase values with the position **q** on the screen. Its goal is to compensate the distortion of the sinusoidal stripes on the screen. The camera calibration is needed to assign the line of sight **v** to each point of the picture **p**. The lens of the camera distorts the ideal pinhole camera model, this is corrected by a correction function. Finally the calibration of geometry translated all coordinates in the common world coordinate system. The position of the camera in the world coordinate system is gathered by the measurement of a special mirror with marks. The marks are positioned on a grid of $4\,\text{mm} \times 4\,\text{mm}$, these position are at known points in the world coordinate system. Knowing the lines of sight and the positions of the marks it is possible to do a resection and find out where the camera is located. This can be done for each camera separately. The position of the screen is gathered in the same way, a resection is done using the mirror with the known marks. More details of the different steps in the calibration process are found in Knauer (2006).

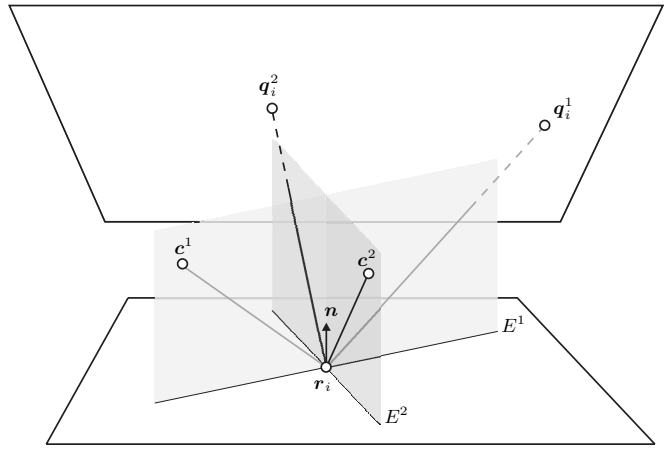

Figure 4.4.: This sketch shows a three dimensional view of the two camera positions, denoted with $\mathbf{c}^1$ and $\mathbf{c}^2$. The lower tetragon is the mirror and the upper one the screen. If the reflecting point $\mathbf{r}$ is moved the potential normals for camera one lay all in plane E^1 and the potential normals for camera two in plane E^2. The only possible normal fulfilling the requirements for both cameras is the intersection line of the to planes; picture from Knauer (2006).

Parameters during the measurement

The first step of the measurement process is to assign the phase φ to a unique position on the screen. But before the pattern has to be projected. The phase of a sine repeats after each interval of $[0, 2\pi[$. To code the screen in a unique way two sines with different frequencies are used. If one pattern has P stripes, while the other has Q stripes the encoding is unique if Q and P are coprime. Using the Chinese remainder theorem one can calculate the phase φ from the two measured phases for the different frequencies. Typical values are P= 7 and Q = 8. But to use only eight stripes over the whole screen is not optimal due to the uncertainty relations described in Knauer (2006). A value close to 100 would be ideal for the setup, but to use values close to 100 is not possible because the noise is too high. Therefore the screen is spilt in several parts where the correlation is unique, the number of parts is the so-called stretchfactor S because S·P and S·Q stripes are projected. The correlation to the different parts can be obtained by a measurement with stretchfactor 1.
The next step is the determination of the position on the screen, for which the phase φ is needed. PMD uses a temporal time shift, where N pictures with shifted phases are projected successively. The intensity is measured in each pixel and for each phase shift separately. The intensity depends on the mean intensity I_0, the contrast K and the

known phase offset φ_s. The intensity in each pixel is:

$$I_s = I_0 \left(1 + K \cdot \cos(\varphi - \varphi_s)\right) \quad s = 1...N \tag{4.2}$$

where s denoted the number of the picture. PMD uses a four-shift-algorithm, i.e. N = 4. We want to calculate the phase φ because it is needed to calculate the normal of the surface. For the detection of errors on the surface the contrast is also important because it depends on the curvature. After some algebra one ends up with the following formula for φ:

$$\varphi = \arctan \frac{I_2 - I_4}{I_1 - I_3} \tag{4.3}$$

with I_i being the intensity in one pixel for picture number i.

After determining the phase and therefore the position on the screen for each pixel the potential normals are calculated. The potential normals for the two cameras are compared and the true normal is the one where the difference between the potential normal for camera one and camera two is minimal. Now the height as well as the normals of the object which is tested are determined.
The curvature is obtained by a numerical differentiation of the slope of the object. Although one in principle gets the height of the object by stereodeflectometry, it is more accurate to integrate the slope values. The lateral resolution of 200 μm leads to a variation in height of 10 nm from pixel to pixel.
The measurement of the focal length (f) is already done by the measurement of the radius of curvature ($R = 2 \cdot f$).

First test

To test whether the structure we see is part of the mirror and not the measurement technique, we rotated the mirror and did several measurements.

In Fig. 4.5 it is shown how the structure rotates together with the mirror. These measurements are done with a single frequency, leading to a striped pattern, which is clearly seen in each of the four pictures. This pattern does not rotate together with the mirror structure but stays in the same direction for all four measurements. To overcome this, the measurement can be done with several frequencies, i.e. a multi-frequency measurement.

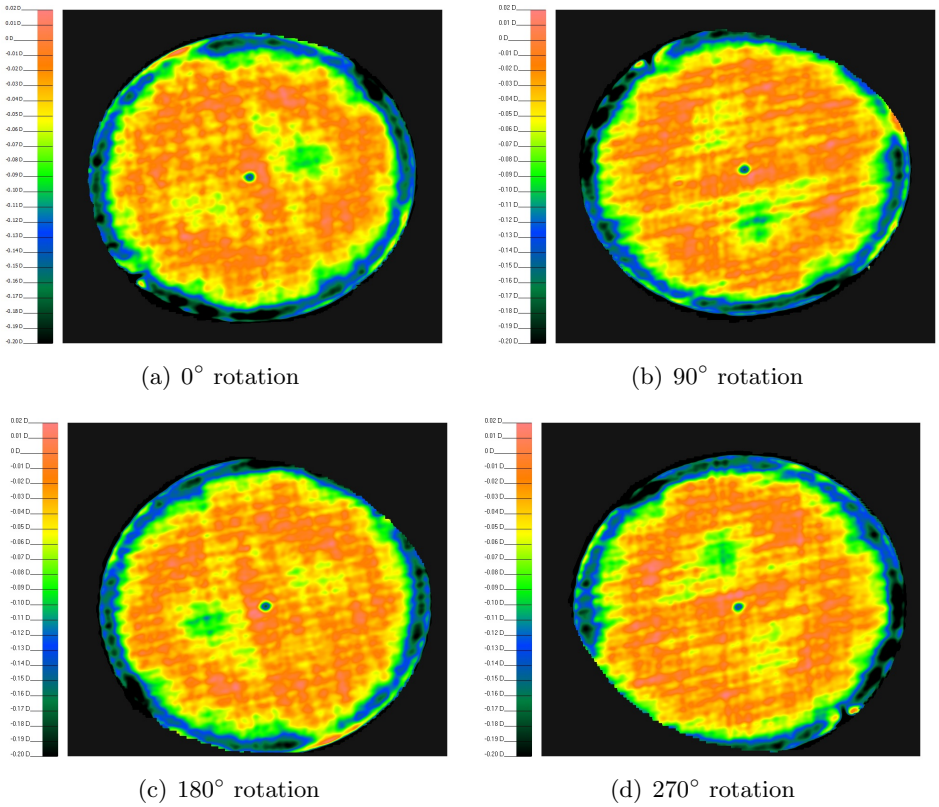

(a) 0° rotation (b) 90° rotation

(c) 180° rotation (d) 270° rotation

Figure 4.5.: The mean curvature of the Cracow glass mirror at different rotation angles.

Multi-frequency measurement

The usual measurement is done with one stretch factor in both directions. This leads unfortunately to distortions on the object, as can be seen in Fig. 4.6(a). The width of these striped pattern depends on the stretch factor only. To overcome this one can do a so-called multi-frequency measurement, for which one defines the start value of the stretch factor, as well as the step and the end value. This leads to an averaging of the stripe pattern. Fig. 4.6 shows the difference between a usual measurement and a multi-frequency measurement. As the stripe pattern is drastically reduced, all following results are obtained using multi-frequency measurements.

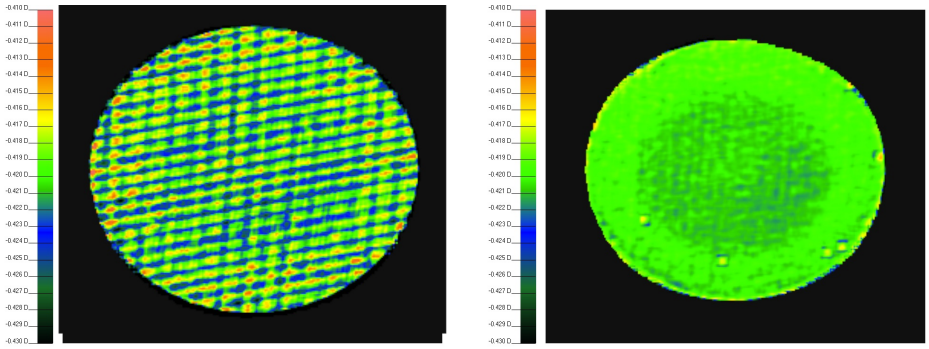

(a) The mean curvature obtained by a single frequency measurement

(b) The mean curvature obtained by a multi-frequency masurement

Figure 4.6.: Comparison of a single and a multi-frequency result for the small H.E.S.S. mirror 1194 mirrror. The mean curvature is color-coded, given in diopter.

Setup

For all measurements described in this thesis we used an existing setup which was developed in the OSMIN group. In Fig. 4.7 the setup is shown, one can see the cameras, the screen and the mirror which is measured.

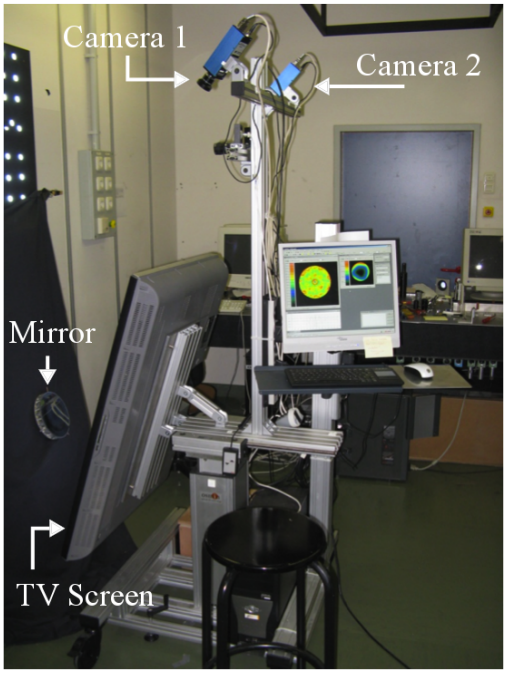

Figure 4.7.: Picture of the PMD setup developed by the OSMIN group.

4.2. Ray tracing

The primary output of the PMD measurement is the slope and the normal data of the mirror's surface, it has to be translated into the PSF by a ray trace simulation. Ray tracing is an algorithm that simulates the path of light rays through an optical system. In our case only the reflection at the surface of the mirror facet is taken into account. Using the shape and the normal data it is possible to get the PSF at arbitrary distances and angles from the mirror facet.

We simulated the incoming rays and reflected them on the surface of the mirror. The reflection was done using the fact that the angle of incidence is the same as the angle of the reflected ray, for which only the normal and the height data of the surface are needed (see Fig. 4.8).

The point spread function is calculated by binning the intersection points of the reflected rays and the plane of interest (where the picture is taken) into a histogram. Two different cases were investigated. The first one is the setup in which the $2f$ measurement is carried out. The point-like light source is placed in a distance of two times the focal length of

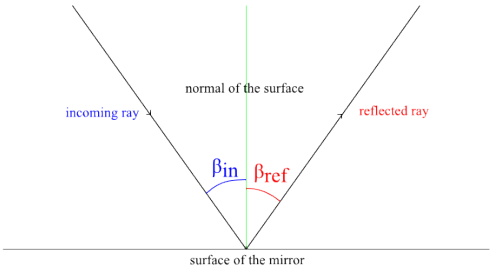

Figure 4.8.: Reflection of an incoming ray, as used in the Matlab script.

the mirror and the picture is taken in the same distance. This is the best way to compare the results obtained by the different methods, $2f$ and PMD.

The second case is the real science scenario, the way the mirror facets are used when they are put on the telescopes. In this situation the light source is at a distance of several kilometres, for which a light source placed at infinity is a good approximation. Hence the incoming rays are parallel rays and the picture is taken in a distance equal to the focal length f.

The ray tracing is implemented into a Matlab[2] script. The surface and the normal data of the PMD measurement are read in. The file format is such that one gets six values for each point on the grid. The six values are the surface and the normal values, both in x,y and z. One can imagine the mirror facet to consist of many small mirror parts (pixels) for which we know the position and orientation.

One important step is to determine the plane in which the mirror lies or the normal of it. This is not trivial because the mirror is spherical. One way to do that is to use three points on the edge of the mirror facet, the cross-product of the vectors connecting these points is perpendicular to the plane defined by the points. A second way is to take the normal in the mirror center and use this as the normal of the complete mirror. If one is able to find the exact center of the mirror this is a good description of the mirror normal. But the determination of the mirror center is also difficult. In the end one can define the optical axis of the system, specified by the mirror center and the normal of the plane.

The light rays are defined by a suspension point and a direction vector. In the case where the light source is at infinity the incident rays all have the normal of the plane as direction

[2]Matlab is a technical computing language and interactive environment for algorithm development, data visualization, data analysis, and numeric computation. See http://www.mathworks.com/products/matlab/.

vector and the suspension points are points on a regular grid in the x- and y-direction. Since we did not want to interpolate between two pixels we chose the suspension points of the incident rays to be the surface points of the measurement. For the $2f$ case the first step is to calculate the position of the light source. The light source is positioned on the optical axes and at a distance of $2f$ of the mirror center. The direction of the incident rays is determined by the line connecting the light source and the surface points, it is different for each pixel. Knowing the incident rays one can calculate the reflection on the surface using the formula:

$$\mathbf{r}_{out} = \mathbf{r}_{\text{in}} - 2 \cdot \mathbf{n} \cdot (\mathbf{r}_{\text{in}} \cdot \mathbf{n}) \tag{4.4}$$

where $\mathbf{r}_t extout$ and $\mathbf{r}_t extin$ are the directions of the outgoing and incoming ray and $\mathbf{n}$ the normal from the measurement.

The outgoing rays are then defined by the surface point as the suspension point and the direction obtained by the calculation above. The PSF is obtained by binning the intersection points of the outgoing rays and the plane at $2f$ or f into a histogram. The simulations of the ray tracing on a perfect sphere demonstrates that the script works fine. In Fig. 4.9 a sample of simulated rays for a perfect sphere with a radius of curvature of 30 m and an edge length of 500 mm is shown for both cases.

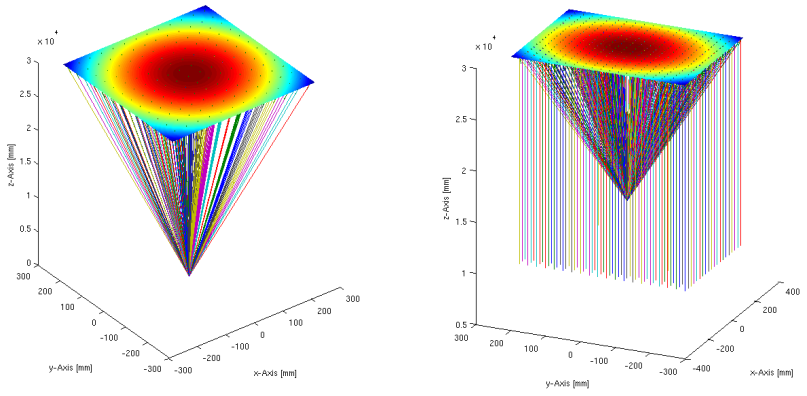

(a) Light source in $2f$, it is hardly possible to distinguish the incoming and outgoing rays.

(b) Light source at infinity, the incoming rays are parallel.

Figure 4.9.: Sample of simulated rays for a perfect sphere.

In this ideal case the intensity distribution, which is the result of the ray tracing, is smaller than 1 μm.

4.3. Steps in the analysis process of PMD

We show the results exemplarily for the two mirrors from Saclay because they are real prototypes for CTA, have a good quality, and have the size we can maximal measure with the current PMD setup. The measurements have been carried out together with Christian Faber and Tamas Gal from the OSMIN group.

The first measured variable is the slope of the object in the x- and the y-direction, shown in Fig. 4.10.

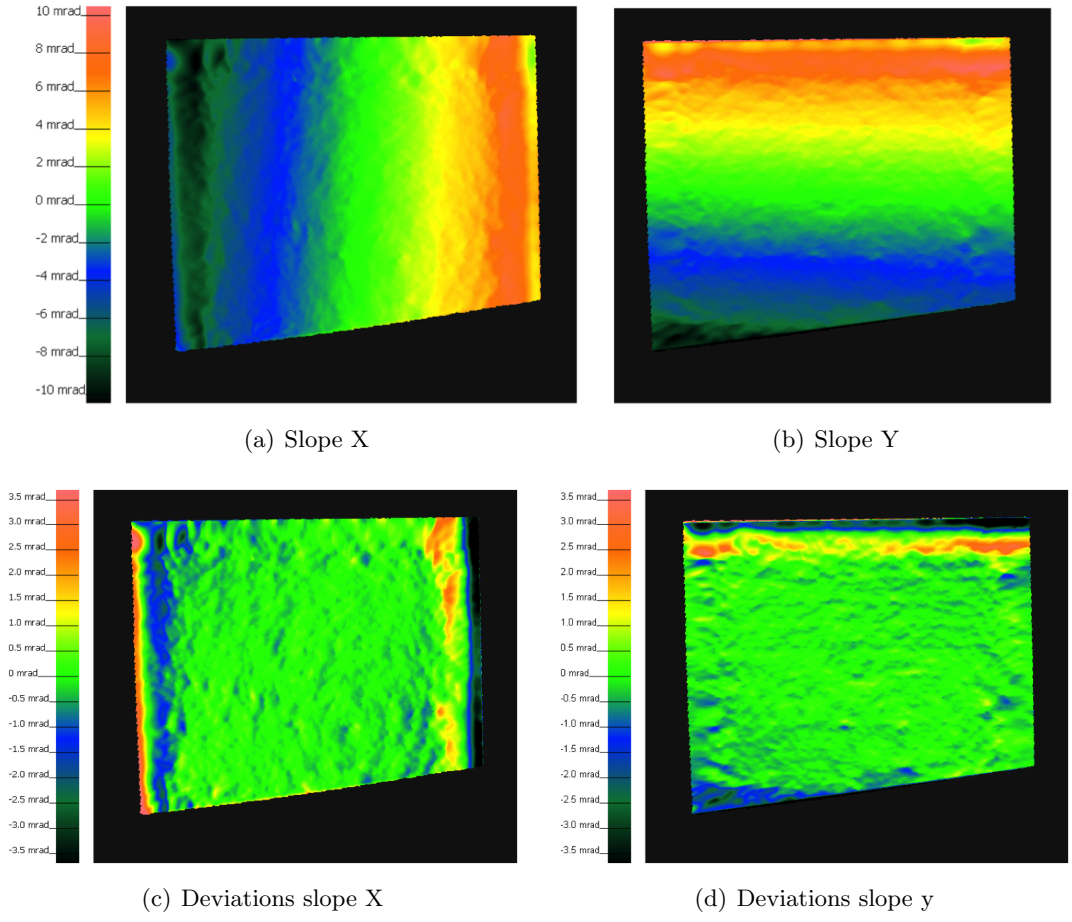

(a) Slope X

(b) Slope Y

(c) Deviations slope X

(d) Deviations slope y

Figure 4.10.: PMD results for the Saclay aluminium mirror. The upper panels show the slope in the x- and y-direction. The lower panel show the results if a tilt is subtracted from the shape.

The dominant feature in Fig. 4.10 is a change from left to right or top to bottom caused by the fact that the cameras do not look straight onto the mirror. However it is possible to subtract the mean tilt, the result is shown in the lower panel of Fig. 4.10. It can be seen that the inner part is smooth, but the are some deviation at the edges.

The shape is obtained by numerical integration of the slope, the results are shown in Fig. 4.11. The left panel, Fig. 4.11(a), shows the shape of the mirror, in the right panel a sphere has been subtracted to see the deviations more clearly. The deviations from the sphere have a range from -40 to $+20\,\mu$m, only the deviations in the upper corners are higher.

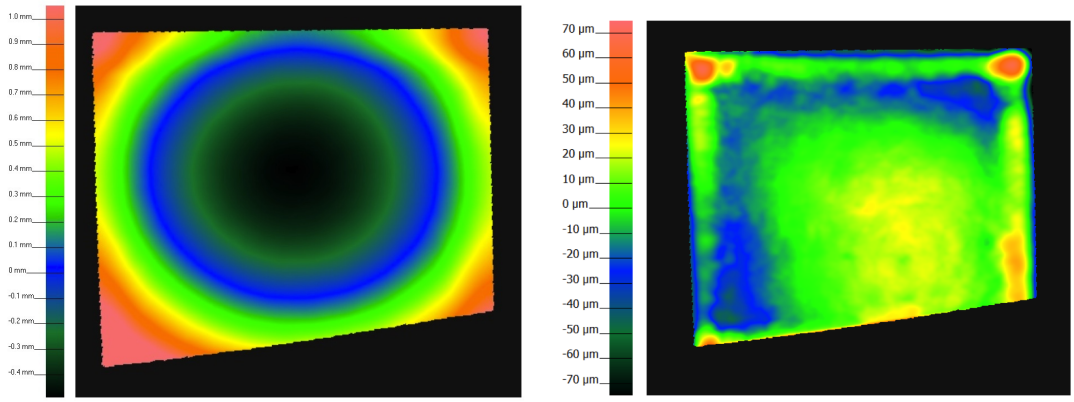

(a) Shape (b) Shape with a sphere subtracted

Figure 4.11.: The shape of the aluminum mirror.

The cross sections of the shape indicated by the dotted lines in Fig. 4.12(a) are shown in Fig. 4.13. They show a nearly perfect spherical shape. In order to evaluate the deviation from the perfect sphere we calculated the sag of the sphere. The sag is the difference in height between the mirror center and another point on the mirror, typically on the edge. The formula for the sag s, with the notations as in Fig. 4.12(b), is:

$$s = R - \sqrt{R^2 - \left(\frac{d}{2}\right)^2}.$$

The Saclay aluminium mirror has a radius of curvature of $R = 30\,\text{m}$ and an edge length of $d = 0.5\,\text{m}$, this leads to an expected sag for cross section 1 of 1.0 mm. The edge length d for cross section 2 is the diagonal and therefore a factor $\sqrt{2}$ larger, leading to an expected sag of 1.5 mm. The cross sections, presented in Fig. 4.13(a) and Fig. 4.13(b), show that the measured sag is in agreement with the calculated one.

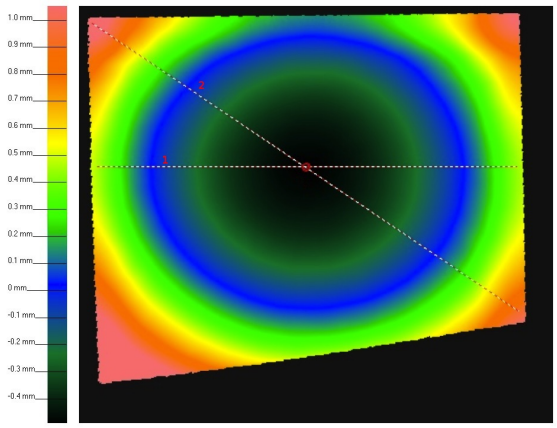

(a) The shape of the aluminium mirror from Saclay. The cross sections shown below follow the dotted lines in this picture.

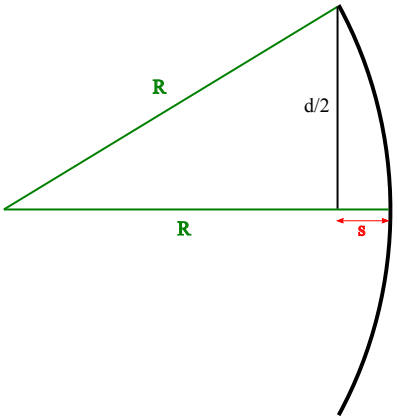

(b) Sketch showing the parameters to calculate the expected sag s. R denotes the radius of curvature of the mirror and d its edge length. Not to scale.

Figure 4.12.: The shape of the aluminum mirror with the cross sections indicated by the dotted lines and a sketch to calculate the sag.

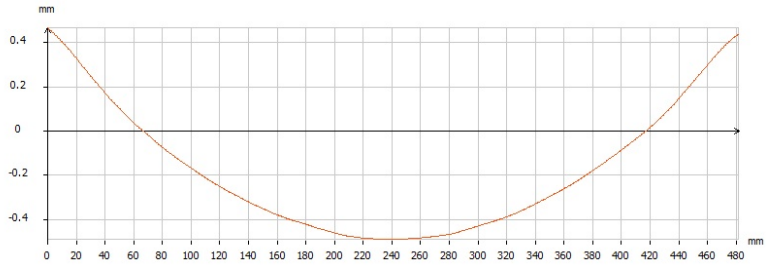

(a) Cross section 1, showing a sag of 1 mm.

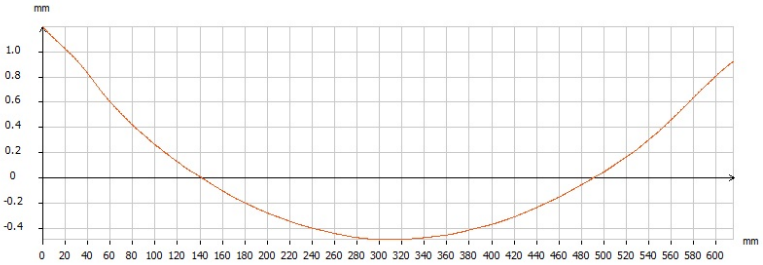

(b) Cross section 2, showing a sag of 1.5 mm.

Figure 4.13.: Cross sections of the shape of the Saclay aluminium mirror.

The mean curvature is obtained by differentiation of the slope, the result for the Saclay mirrors are shown in Fig. 4.14. In eyeglass manufacturing processes the curvature is usually expressed in diopters, the reciprocal of the radius of curvature. The sign of the diopter value represents the orientation of the curvature, negative is convex and positive is concave. As PMD was originally developed for eyeglass measurements the software we used also expresses the curvature in diopters. For a nominal focal length of 15 m the nominal diopter value is $\Phi = -0.0333\,\mathrm{D}$.

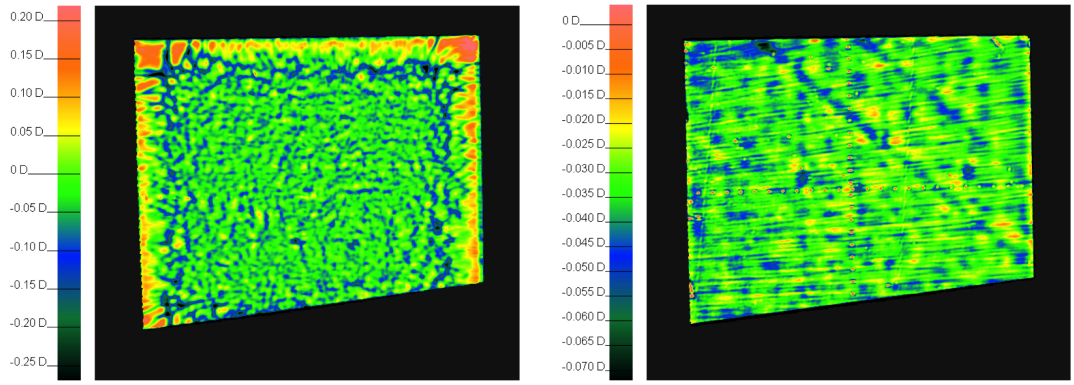

(a) Aluminium mirror (b) Carbon mirror

Figure 4.14.: The mean curvatures for the Saclay mirrors, note that the range of the color-code is not the same.

The average mean curvature c_{mean} of the complete aluminium mirror is $\approx -0.03\,\mathrm{D}$ with a standard deviation $\sigma = 0.09\,\mathrm{D}$. If calculated for the inner part only, $\overline{c_{\mathrm{mean}}} \approx -0.03\,\mathrm{D}$ with $\sigma = 0.03\,\mathrm{D}$. The mean value is close to the expected one, but as seen by the large σ, many parts of the mirror have a large deviation from the expected curvature.

The values for the carbon mirror are much better: for the whole mirror $\overline{c_{\mathrm{mean}}}$ is $-0.034\,\mathrm{D}$ and σ is $0.007\,\mathrm{D}$. Note that the range of the color code is different, for the aluminium mirror shown in Fig. 4.14(b) it is $0.45\,\mathrm{D}$, while for the Carbon mirror shown in Fig. 4.14(a) the range is only $0.07\,\mathrm{D}$.

Using the shape and the normal data one can use the ray tracing script to calculate the PSF. The result of the ray tracing for the aluminium mirror is shown in Fig. 4.15(a).

The result of the ray tracing looks reasonable and has the same size as the $2f$ result. The comparison of the PSFs obtained by the two different methods is done in detail in Chapter 5. This ray tracing result shows that it is possible to calculate the PSF of a mirror facet from the shape and normal data gathered by a PMD measurement.

Table 4.1.: The characteristic values obtained by the PMD measurement for the Saclay aluminium mirror.

Direction	Aluminium mirror			Carbon mirror		
	σ [mm]	d_{80}^{length} [mm]	d_{80}^{angle} [mrad]	σ [mm]	d_{80}^{length} [mm]	d_{80}^{angle} [mrad]
x-direction	25	64.5	2.15	7	18.1	0.60
y-direction	20	51.6	1.72	16	43.9	1.46

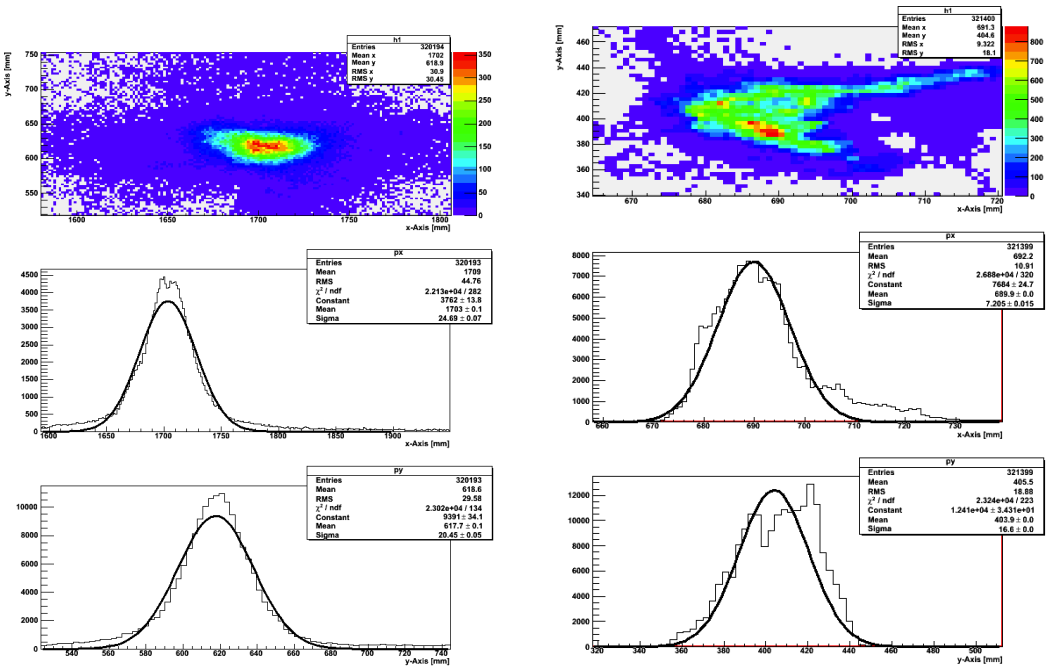

(a) PSF of Saclay aluminum

(b) PSF of Saclay carbon

Figure 4.15.: Ray tracing results for the Saclay mirrors

The ray tracing results for the carbon mirror are shown in Fig. 4.15(b), the values for the Gaussian fit are given in Tab. 4.1. In Fig. 4.15(b) in the upper most panel it can be seen that fit to the projection in the y direction is not good. One reason might be, that if a relatively low intensity is spread over a large area this is not detected by the $2f$ setup due to the background. In the ray tracing script many small values can add up to a large value in the projections.

4.4. PMD results for different mirrors

H.E.S.S. test mirrors 1194 and 641

These mirrors were small test mirrors for H.E.S.S. and were analyzed because they were characterized in detail by measurements done in Heidelberg. The results for the mean curvature and the deviations from the sphere are shown in Fig. 4.16 and Tab. 4.2 shows the results for the Gaussian fits.

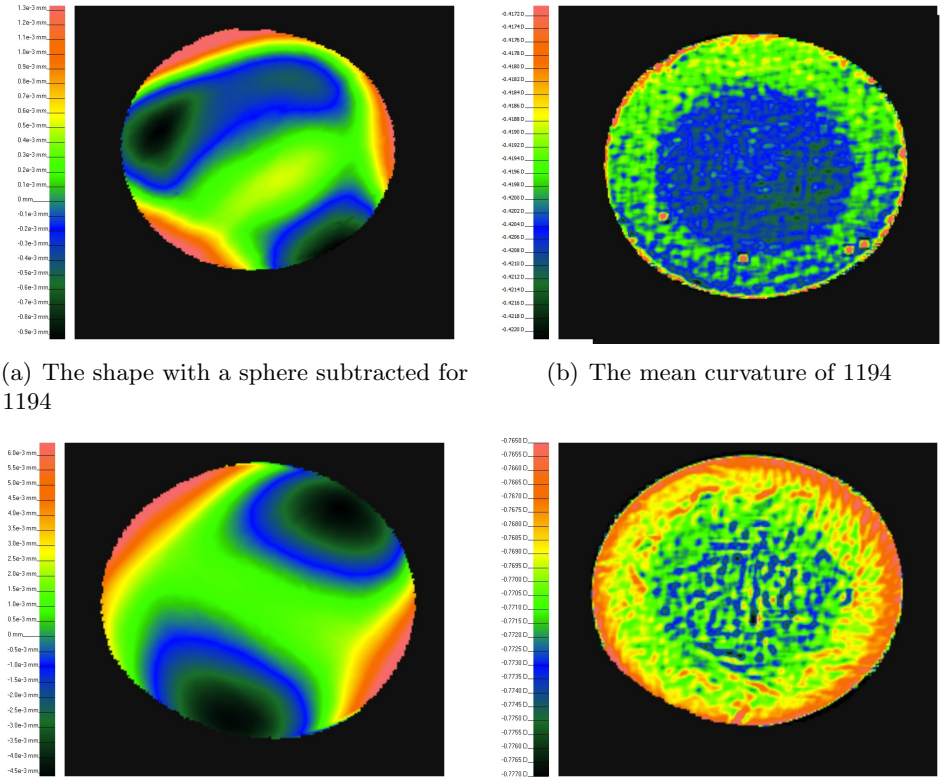

(a) The shape with a sphere subtracted for 1194

(b) The mean curvature of 1194

(c) The shape with a sphere subtracted for 641

(d) The mean curvature of 641

Figure 4.16.: The PMD results for the small H.E.S.S. test mirrors 1194 and 641.

The left panels in Fig. 4.16 show the deviations from the sphere for both mirrors. In the ideal case these deviation would be 0, for mirror 1194 the mean value is $-8 \times 10^{-3}\,\mu$m with a standard deviation σ of $0.4\,\mu$m. Mirror 641 has a mean deviation of $3 \times 10^{-2}\,\mu$m and a standard deviation σ of $2\,\mu$m. Both values show the high quality of the small H.E.S.S.

Table 4.2.: The characteristic values obtained by the PMD measurement for the small H.E.S.S. mirrors.

Direction	Mirror 1194			Mirror 641		
	σ [mm]	d_{80}^{length} [mm]	d_{80}^{angle} [mrad]	σ [mm]	d_{80}^{length} [mm]	d_{80}^{angle} [mrad]
x-direction	0.13	0.34	0.20	0.73	1.88	1.47
y-direction	0.19	0.49	0.21	0.62	1.60	1.25

Table 4.3.: The average mean curvatures obtained by the PMD measurement for the small H.E.S.S. test mirrors. The units are diopter.

c_{mean}	Expected value	Mean measured value	Range of the measured values
H.E.S.S. 1194	-0.419	-0.420	0.006
H.E.S.S. 641	-0.780	-0.77	0.06

mirrors, as in the other measurements mirror 1194 is slightly better than mirror 641.

To compare the values for the focal length one has to calculate the values for the average mean curvature, the results for both small H.E.S.S. mirrors are shown in Tab. 4.3. The measured values are in very good agreement with the expected ones. The PSFs for both mirrors are obtained by using the ray tracing script. The result is shown in Fig. 4.17.

H.E.S.S. A153

The current PMD setup is not large enough to be able to measure the complete H.E.S.S. mirror A153. Thus we measured only part of the mirror, the mean curvature is shown in Fig. 4.18(a). Note that the scale for the color-coding is different for the other measurements. For a radius of curvature of 30 m one would expect a mean curvature of -0.033 D. The average mean curvature is -0.0339 ± 0.0005 D. The small curvature is difficult to measure, but the result shows the high quality of the H.E.S.S. mirrors.

The ray tracing result is shown in Fig. 4.18(b). The values from the Gaussian fit are shown in Tab. 4.4. The values are good, but they cover only the PSF of half the mirror. A difficulty in the ray tracing was the determination of the mirror center and the plane the mirror lies in. We are currently working on the design and construction of a larger setup to measure also larger mirrors.

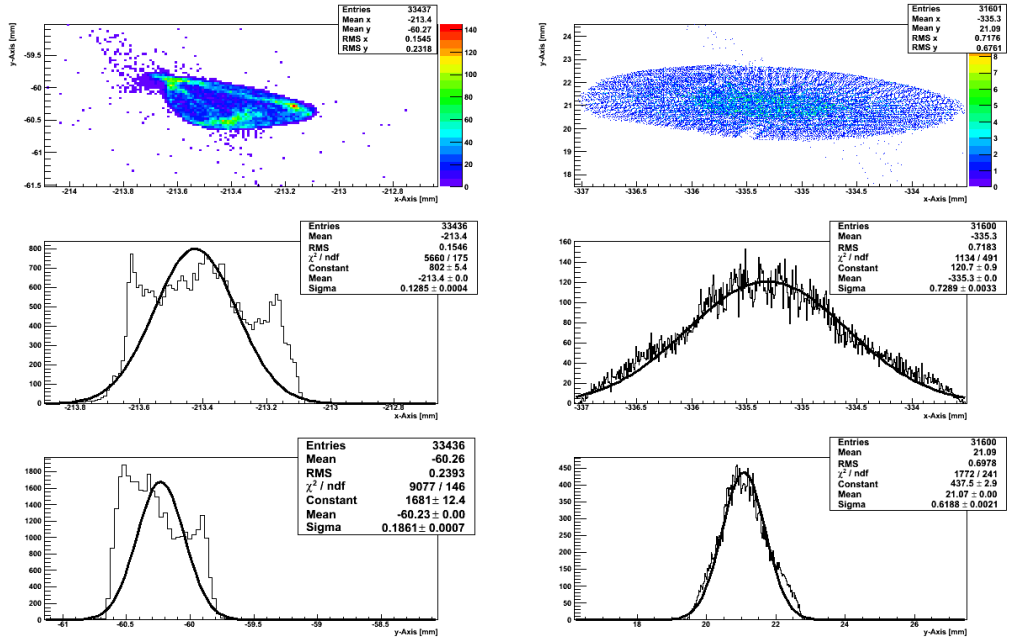

(a) PSF of 1194 (b) PSF of 641

Figure 4.17.: The ray tracing result for the small H.E.S.S. mirrors.

Table 4.4.: The characteristic values obtained by the PMD measurement for part of the H.E.S.S. A153 mirror.

Direction	σ [mm]	d_{80}^{length} [mm]	d_{80}^{angle} [mrad]
x-direction	9.8	25.3	0.84
y-direction	5.3	13.6	0.45

Mirrors from Cracow

Another prototype for CTA mirrors are the Cracow mirrors, we measured them with PMD and got the results shown in Fig. 4.19.

The average mean curvature of the epoxy mirror is $\overline{c_{\text{mean}}} = -0.036\,\text{D}$, with a range of 0.18 D, of the glass mirror is $\overline{c_{\text{mean}}} = -0.034\,\text{D}$, with a range of 0.11 D. Both are compatible with the expected value of 0.033, however in the right panels of Fig. 4.19 prominent deviations can be seen.

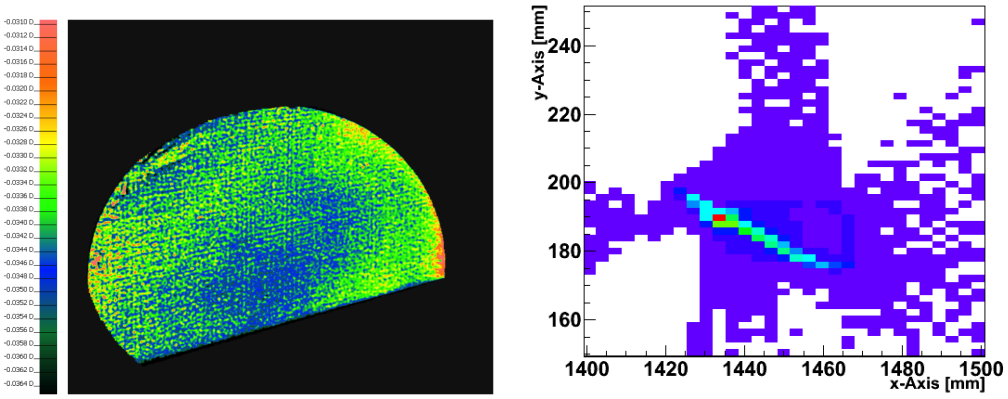

(a) The mean curvature

(b) The raytracing result

Figure 4.18.: The PMD results for the H.E.S.S. A153 mirror. The left panel shows the mean curvature and the right panel the PSF obtained by ray tracing.

Table 4.5.: The characteristic values obtained by the PMD measurement for the Cracow epoxy mirror.

Direction	Epoxy mirror			Glass mirror		
	σ [mm]	d_{80}^{length} [mm]	d_{80}^{angle} [mrad]	σ [mm]	d_{80}^{length} [mm]	d_{80}^{angle} [mrad]
x-direction	20.15	51.99	1.73	24.34	62.80	2.09
y-direction	12.45	32.12	1.07	20.76	53.56	1.79

The deviations from the sphere for the epoxy mirror have a mean value of $(8 \pm 70) \times 10^{-4}$ mm. The deviations from the sphere for the glass mirror have a mean value of $(1 \pm 10) \times 10^{-3}$ mm. This is close to the ideal value of 0, although one can see in the left panels of Fig. 4.19 that the deviations are stronger on the edges.

The PSF of both mirrors is obtained by using the ray tracing script. The results are shown in Fig. 4.20(a) and Tab. 4.5.

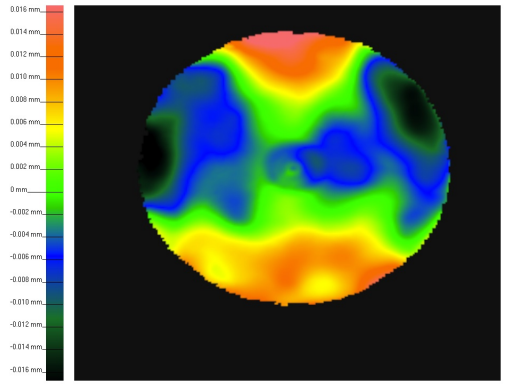

(a) The shape with a sphere subtracted for the epoxy mirror.

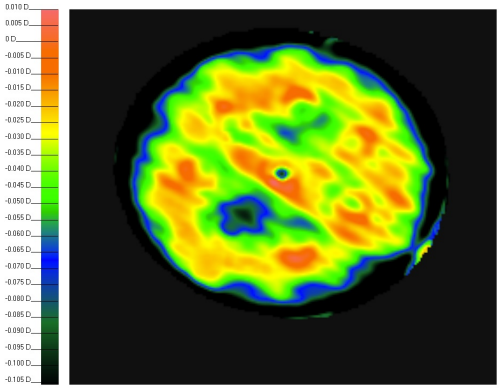

(b) Mean curvature for epoxy

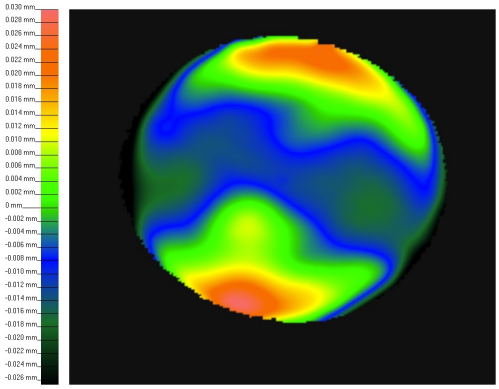

(c) The shape of the mirror with a sphere subtracted for the glass mirror

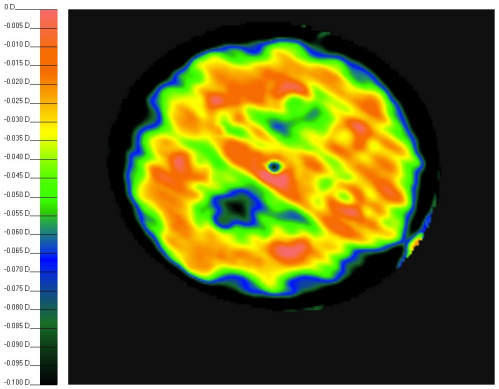

(d) Mean curvature for glass

Figure 4.19.: The PMD results for the Cracow mirrors. The left panels show the deviation from a sphere and the right panels shw the mean curvature.

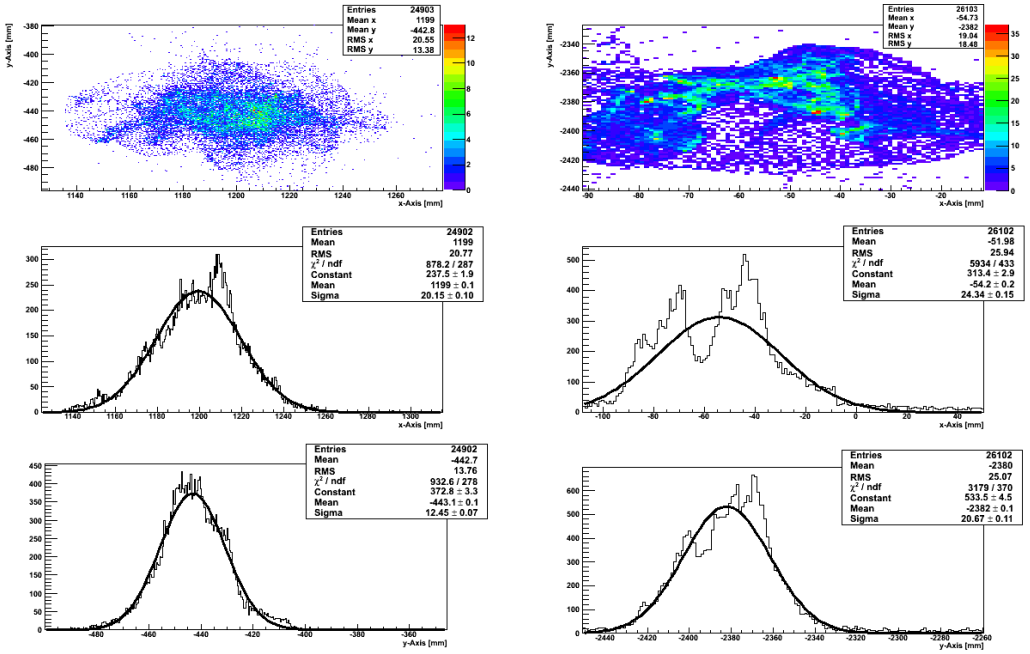

(a) PSF of the epoxy mirror

(b) PSF of the glass mirror

Figure 4.20.: The ray tracing results for the Cracow mirrors.

5. Comparison of the two methods

In this Chapter we present the results for the PSFs of different mirrors, obtained with the two different techniques. The results of the raytracing and the $2f$ method are compared directly with each other.

Focal length

One parameter which was measured for the H.E.S.S. mirrors with both techniques is the focal length. A comparison is shown in Tab. 5.1. The obtained values do agree nicely with each other for all three mirrors, as well as with the nominal value. Both methods include the possibility to measure the focal length. The determination of the focal length has in both setups smaller errors for shorter focal lengths. In the $2f$-case this is due to smaller distances. For the PMD method it is also easier to measure mirrors with shorter focal length since the curvature is larger. For the H.E.S.S. A153 mirror the expected value for the curvature is 0.033 D, even a change in the order of 0.001 D leads to a large difference in the focal length.

The determination of the focal length is in any case not the most important parameter, since the only size which is crucial when the mirrors are mounted is the size of the PSF at the nominal focal length.

Table 5.1.: Comparison of the focal length values for different methods.

Mirror	$2f$ [m]	PMD [m]	Nominal [m]
H.E.S.S. A153	14.9	14.9	15.0
H.E.S.S. 1194	1.182	1.185	1.194
H.E.S.S. 641	0.642	0.645	0.641

Point spread function

The determination of the point spread function is the most important goal of the test. Figure 5.1 shows the results for the small H.E.S.S. test mirrors. The range of the axes is different: for the 1194 mirror it is 2.5 mm, for the 641 mirror it is 4 mm. The results for the different measuring techniques have the same size, but the detailed structure is not the same. For PSFs smaller than 1 mm several factors have to be taken into account, e.g., the expansion of the light source and the calculation of the plane the mirror lays in.

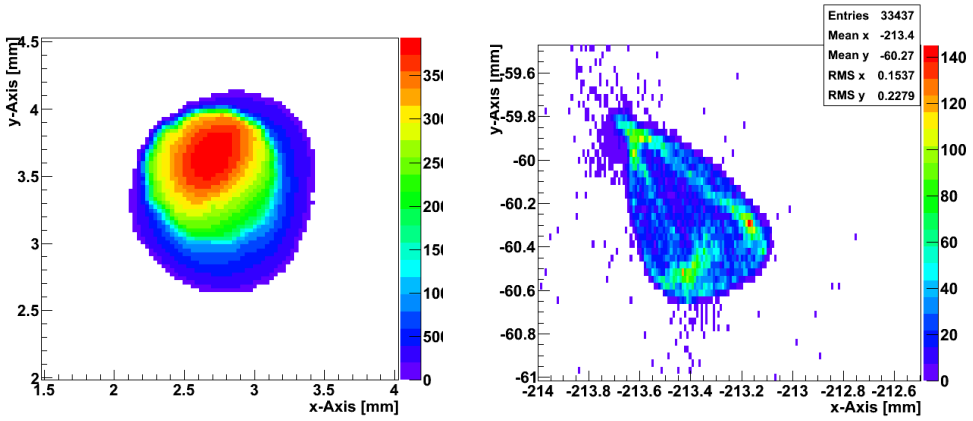

(a) PSF from $2f$, 1194

(b) PMD raytrace result, 1194

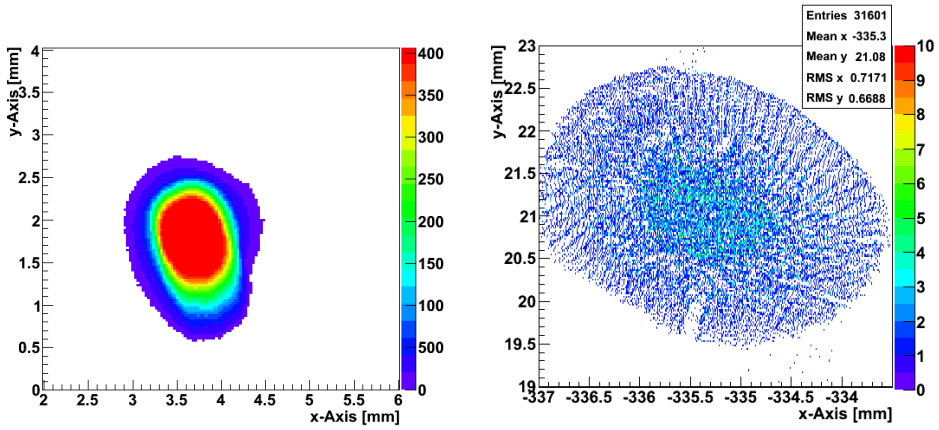

(c) PSF from $2f$, 641

(d) PMD raytrace result, 641

Figure 5.1.: Comparison of the results obtained for the H.E.S.S. 1194 (upper panels) and 641 (lower panels) by a $2f$ and a PMD ray-trace measurement.

The decision whether a mirror stands the proof for CTA will never be in question if its PSF is smaller than 1 mm, therefore the determination of such small features is not crucial. We will nonetheless investigate these features further, but this is beyond the scope of this thesis.

In Fig. 5.2 the two results for the aluminium mirror from Saclay are shown. The size is the same for the different measurements and there are no special features in any picture. The aluminium mirrors from Saclay do not fulfil the specifications for CTA.

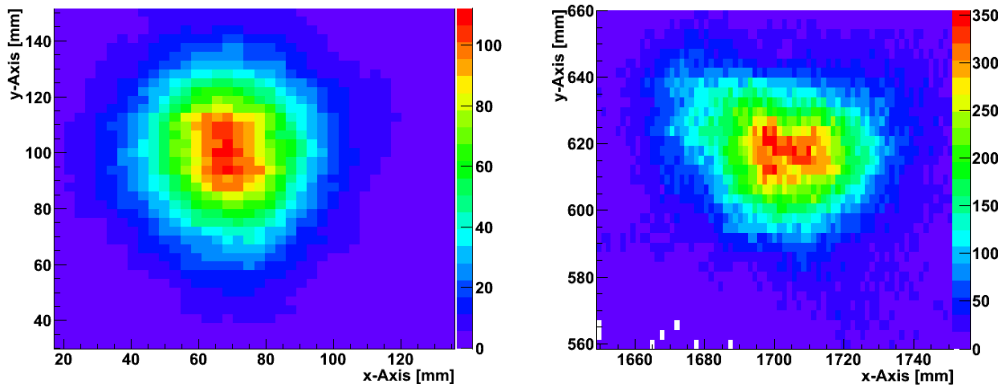

(a) PSF from $2f$

(b) PMD raytrace result

Figure 5.2.: Comparison of the results obtained for the Saclay aluminium mirror by a $2f$ and a PMD ray-trace measurement.

The results for the Carbon mirror from Saclay are better than for the aluminium mirror, they fulfil the requirements for CTA. The $2f$ measurement was carried out by Clementina Medina in Saclay. As can be seen in Fig. 5.3, the size of the PSF is about the same, although the $2f$ measurement shows a smaller extension in the y-direction. This might be due to the higher background.

Figure 5.4 shows the comparison of the PSFs of the Cracow glass mirror. The size is the same, but the small features look different. It is very likely that these features originate from small surface structures and are wavelength-dependent. The three measurements are carried out at different wavelengths.

The results for the Cracow epoxy mirrors, shown in Fig. 5.5, are promising, even though the PSFs are too large to fulfil the CTA specifications at the moment. The PSFs look very similar for the different techniques. The pictures match nicely if the $2f$ measurement is flipped vertically. We will further investigate this feature.

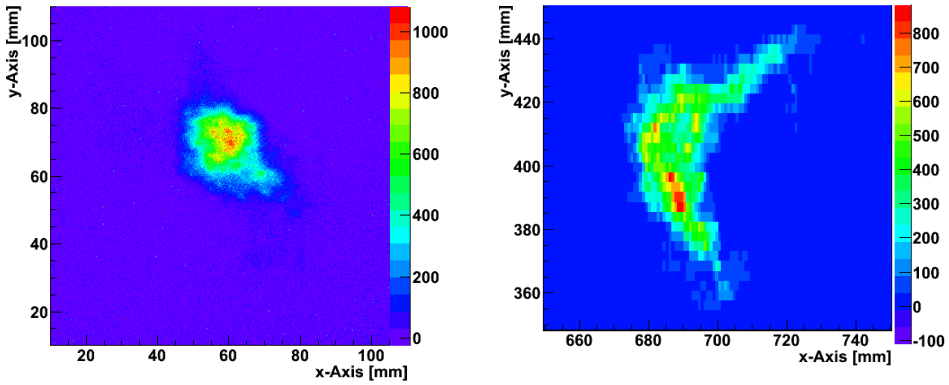

(a) PSF from $2f$, Clementina's result

(b) PMD raytrace result

Figure 5.3.: Comparison of the results obtained for the Saclay carbon mirror by a $2f$ and a PMD ray-trace measurement.

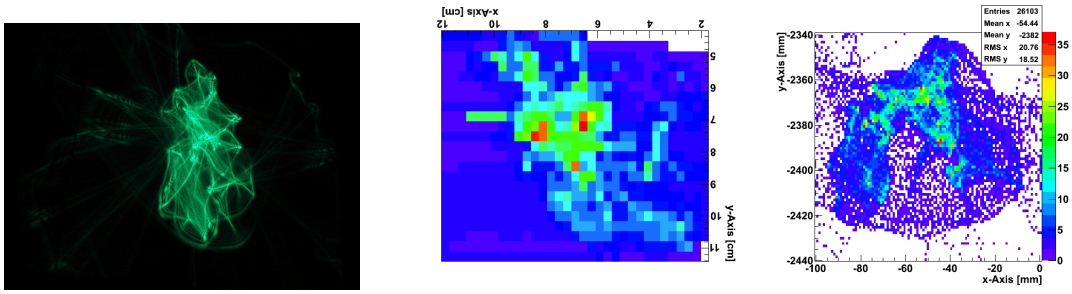

(a) Picture taken with a digital camera, green laser, flipped vertically

(b) Scan result, red laser, flipped vertically

(c) PMD ray-trace result

Figure 5.4.: Comparison of the results for the Cracow glass mirror obtained by a $2f$ and a PMD ray-trace measurement.

In any case the homogenity of the result is astonishing, as can be seen in Fig. 5.5.

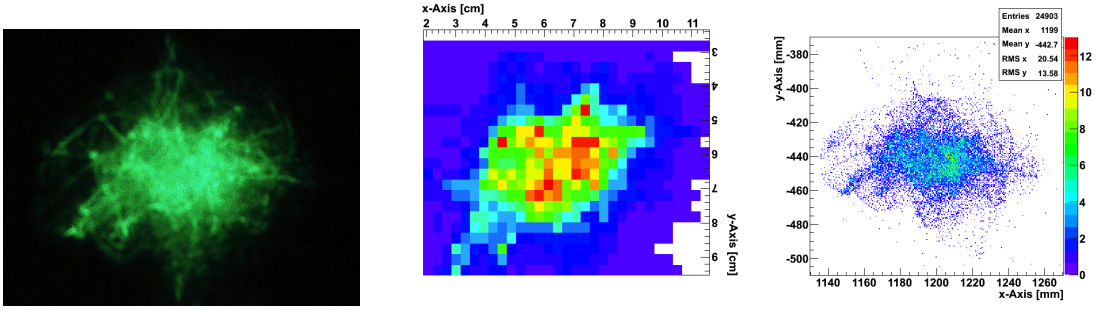

(a) Picture taken with a digital camera, flipped vertically

(b) Scan result, red laser, flipped vertically

(c) PMD raytrace result

Figure 5.5.: Comparison of the results obtained for the Cracow epoxy mirror by a $2f$ and a PMD Raytrace measurement.

Mirror	$2f$ [mm]		PMD [mm]	
	x-axis	y-axis	x-axis	y-axis
H.E.S.S. A153	1.63	1.36	9.8†	5.3†
H.E.S.S. 1194	0.28	0.27	0.13	0.19
H.E.S.S. 641	0.26	0.40	0.73	0.62
Saclay carbon	6.6*	7.9*	7.2	16.6
Saclay aluminium	16.5	20.9	24.7	20.5
Cracow epoxy	18.5	13.9	20.2	12.5
Cracow glass	20.4	24.0	24.3	20.8

Table 5.2.: Comparison of the σ values for different methods. † only part of the mirror was used for this measurement. * these measurements are obtained by a $2f$ measurement from Clementina Medina.

The values for the σ in x- and y-direction for the two methods (see Tab. 5.2) are compared in Fig. 5.6. The systematic error is estimated to be 1 mm for all measurements. The red crosses denote the measurements we did, the blue filled circles are points for which only the PMD measurement was done by us, but the $2f$ measurement was done by Clemetina Medina in Saclay. For this comparison the values for the H.E.S.S. A153 were not used, since we could only measure part of the mirror with PMD.

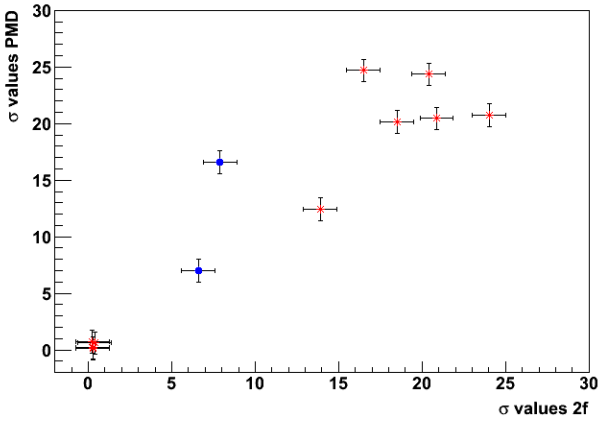

Figure 5.6.: Result for the correlation between σ_{PMD} and σ_{2f} assuming an error of 1 mm for both techniques. The red crosses are values where we performed both measurements, the blue circles indicate that the $2f$ measurement was done in Saclay.

The results correlate nicely. The PMD with the ray tracing script gave in most measurements very similar results as the $2f$ measurements.

6. Conclusion and outlook

We investigated two different methods to characterize mirror facets for the CTA telescopes. The $2f$ method leads to a direct measurement of the PSF of a mirror facet. We found that an optimal setup is obtained by using the LED as light source and the small photodiode or the Adimec camera as detector.

For CTA the decision about the technology to manufacture this enormous amount of mirror facets is still open. Especially during the development phase more detailed information about the surface's texture would be helpful, which can be provided by PMD.

The investigation whether the PMD method is suited to characterize mirror facets for CTA was successful. We measured mirror prototypes with a size up to 50 cm and gained precise information about the surface and the deviations on it. These results can be used to further optimize the manufacturing process. The ray tracing of the PSF was also very fruitful, we managed to calculate the PSF of a mirror by using only the shape and the normal data of it.

The comparison with the $2f$ results show that the PMD is a useful method to investigate characteristics of mirror facets of IACTs. The PMD method has several advantages over the $2f$ setup, like the compact setup, the more detailed information, and possibility to measure without a perfect alignment of the mirror. The achieved precision is high enough. The ray tracing also includes many new possibilities, for example the incoming rays can be simulated on- and off-axis.

Both Saclay mirrors are manufactured with the same technique, only the core material is different. The result from our measurements shows that the carbon structure seems to be better suited.

The maximum size of mirrors we can measure with one shot is, with the current setup,

limited to 50 cm. One possibility to measure larger mirrors would be to do several measurements and stitch them together. The difficulty of stitching is that one needs the absolute height values of the different parts. The absolute height measurement is not precise enough to stitch the different part together without steps in the shape of the mirror. We are working on a new setup which will allow us to measure 1.2 m large mirrors with one shot.

An additional question is the temperature dependence of the mirror facets. The telescopes have no shelter and a typical temperature range the mirrors have to sustain is $-10°$ to $+40°$ C. To make sure that the mirrors do not lose imaging quality with higher or lower temperature, temperature tests are planed. Especially the composite mirrors may get problems due to different expansion coefficients of different materials. This is really difficult to realize in the $2f$-setup since it is not possible to cool or heat a 30 m long corridor. The compact PMD setup includes the possibility to measure in climate chambers. At the moment we are investigating how such a climate chamber setup could be realized. Due to the expansion of the setup structure with temperature it will probably be necessary to calibrate the setup for each temperature.

Overall PMD has proven to be a validable metrology to investigate all properties of IACT mirrors. We are confident that our measurement will help to choose the best possible mirror facets for CTA and thereby ensure a cost-efficient, highly precise instrument.

A. Appendix

List of Figures

List of Tables

B. References

Bibliography

Aharonian F., Akhperjanian A.G., Bazer-Bachi A.R., et al., 2006, ApJ 636, 777

Antonelli L.A., Blasi P., Bonanno G., et al., 2009, ArXiv:0906.4114

Bernlöhr K., Carrol O., Cornils R., et al., 2003, Astroparticle Physics 20, 111

Brun P., 2010, Developement of mirrors in Saclay, priv. comm.

Chaves R.C.G.e.a., 2009, ArXiv:0907.0768; for the H. E. S. S. Collaboration

Cornils R., Gillessen S., Jung I., et al., 2003, Astroparticle Physics 20, 129

CTA Consortium T., 2010, ArXiv:1008.3703

Doro M., 2010, All-aluminium mirrors from the INFN-Padova group, talk at the Liverpool SST meeting 2010

Elfahem S., 1999, Master's thesis, Max-Planck-Institut für Kernphysik in Heidelberg

Giavitto G., 2007, Master's thesis, University of Trieste and Max-Planck-Institut for Nuclear Physics of Heidelberg

Hinton J., 2009, New Journal of Physics 11, 055005

Knauer M.C., 2006, Ph.D. thesis, Universität Erlangen-Nürnberg

Schreiber E., 2005, Master's thesis, Max-Planck-Institut für Kernphysik in Heidelberg

Siemens AG 1997, Silicon NPN Phototransistor SFH 309, Technical report, Siemens, Semiconductor group

Siemens AG 1998, Silicon PIN Photodiode SFH 206 K, Technical report, Siemens, Semiconductor group

Weekes T.C., Cawley M.F., Fegan D.J., et al., 1989, ApJ 342, 379

Acknowledgement

I would like to thank all people who spent their time and shared their knowledge to help me completing my thesis with the best possible result. I especially like to thank:

Christian Stegmann for his infectious enthusiasm for the field of work, the interesting subject of this thesis, and for always having an open ear.
The H.E.S.S. group Erlangen, for a great work climate and enjoyable as well as subject-specific coffee breaks.
Friedrich Stinzing for his supervision, the continuous support, many helpful advices and the proofread of this thesis.
I am grateful for the fabulous support of the OSMIN group under the direction of Prof. Gerd Häusler. Especially Christian Faber, who answered all upcoming questions with awaking enthusiasm and managed to explain things clearly and simply. Furthermore Tamas Gal and Roman Krobot for constantly being ready to help and deeply committed to this project. Not to forget Ondrej Hybl who provided us with a CCD camera and self-made LED including support.
Michi and Markus for the nice coffee breaks and bureau talks.
Sebastian for the help with the convolution and many tips in general.
A special thank to Kora for many interesting discussions on the way to and at work, the patience while learning theoretical physics together, as well as a fabulous time in Namibia.
I wish to thank Luzi for helping me get through difficult times, and for all the emotional support, entertainment, and caring she provided.
My deepest gratitude goes to my parents, brothers, and sisters for their everlasting encouragement and faith in me.
Last but not least I want to thank Felix for his timeless encouragement, his patience, and his love. His limitless help on every possible level makes him irreplaceable. I would have been lost without him.

Persönliche Erklärung

Hiermit erkläre ich, dass ich die Arbeit selbstständig angefertigt und keine anderen als die angegebenen Hilfsmittel verwendet habe.

Erlangen, im November 2010

Anneli Schulz